This is the Author Accepted Manuscript of an article published in Progress in Physical Geography: Earth and Environment. The final authenticated version is available online at: DOI: 10.1177/03091333261480927

Worldwide water gaps

Using relative elevation modelling to identify transverse drainages

Jacqueline Lee

Lee_Jacqueline@outlook.com

Abstract

Transverse drainages are stream reaches that flow through, rather than around, topographic high grounds. The development of transverse drainage is intimately tied to the tectonic history of an area, but the identification of transverse reaches has historically been a matter of subjective opinion. Here, a GIS-based method is presented that uses relative elevation modelling to identify and quantify transverse stream reaches. The process was used on a set of 6557 streams from the World Wildlife Fund's RiverATLAS digital dataset to identify over 7000 potential transverse reaches, of which almost 4000 were visually verified, accounting for over three quarters of the total potential transverse drainage length. The results were used to analyze current theories of formation of transverse drainages on the lower Congo River. The database transverse drainages and geomorphologic analysis are more consistent with an overflow origin for the lower Congo than for stream capture.

The results are viewable online at watergaps.com and are available by emailed request as geopackage and Google Earth KMZ files, along with a Google Earth Sea Level Rise slider that simulates sea level rise, to help visualize the lower elevations of upstream areas that define transverse drainage. The methodology is easily scalable depending on the resolution desired for analysis, and can be helpful in identifying previously undocumented transverse drainage and in expanding the identification and quantification of transverse reaches in areas where transverse drainage is already known to exist.

Keywords

Transverse drainage, water gap, relative elevation modelling, RiverATLAS, Congo River

INTRODUCTION

Transverse drainages are unusual river patterns that flow across topographic high grounds rather than following the seemingly easier path around them (Stokes et al., 2008). They contradict the common expectation that rivers typically begin in mountains instead of flowing entirely through them (Larson et al., 2017).

Water gaps are specific openings through geological features like faults, folds, plateaus, or mountain ranges. They have different regional names worldwide: "cluses" in France, "kloofs" in South Africa, and "tangs" in Iran's Zagros Mountains. Many famous gorges qualify as water gaps, including Tiger Leaping Gorge in China, the Grand Canyon of Arizona, the "Iron Gates" of the Danube River between Romania and Serbia, and the Columbia River gorge through the Cascade Mountains. In this study, the term "transverse drainage" or "TD" encompasses all structural breaches from single water gaps through individual ridges to river pathways crossing entire mountain ranges (Lee, 2021).

Transverse drainages have long served as important transportation corridors through mountainous terrain and as ideal locations for hydropower dams. From a research perspective, the existence of discordant drainage may indicate that past drainage reorganization has occurred, resulting in changes in the direction, quantity and composition of sediment transport from source to sink, and rendering more difficult the task of accurately reconstructing the evolution of continental topography (Heins, 2023; Fernandes et al., 2019; Roberts et al., 2019). Alternatively, discordant patterns may indicate that rivers have overcome tectonic or other influences to maintain their current drainage pattern.

Geologists have been intrigued by TDs since the mid-nineteenth century. For example, Irish geologist H. B. Medlicott, who co-authored with W.T. Blanford the Manual of the Geology of India (1879) and who is credited with coining the term “Gondwanaland,” noted in 1864 that many river courses in the Sub-Himalayas deviated significantly from the underlying rock structure:

> "At innumerable places on every river and stream, we may find instances of the deliberate contravention of this apparently necessary law of natural selection as applied to river courses, and which breaches of law may safely lead us to infer very remote conditions of the surface, very different from what is now apparent. As examples of this, I may mention the case of the Blini [present-day Balaina Nadi], where its course turns out of the band of soft nummulitic strata to cut a narrow gorge across the strike of the hard Infra-Krol rocks, to fall again, after two more bends, into the course of the same valley of rocks. The Sutlej at Bubhor [probably present day Bakhra] gives another instance of the same kind. It cuts a narrow defile across the Naina Devi ridge, which is composed of comparatively hard rocks, in which no sign of crack or bend is traceable, whereas it might apparently,

with much less trouble, have made its way round the point of the ridge, continuing throughout in the softer upper rocks."

Given their importance in the formation of watersheds, the number and location of TDs should be an important consideration when analyzing the drainage history of a given watershed. However, transverse drainages are very difficult to characterize, either quantitatively or qualitatively. In a database of over 1000 articles dating back to 1861 (Appendix A), the only published classification system for TDs is that of Douglass et al. (2009), which uses stratigraphy, plan view, and lithologic features to assign a possible method of formation but does not specify the physical criteria that should be used to distinguish a transversely flowing stream from one flowing in accordance with structure. It appears that the recognition of transverse drainages is primarily a matter of subjective opinion and not of objective criteria.

In an effort to remove some of the subjectivity inherent to TD identification, Lee (2013) suggested that two mappable characteristics can be used to distinguish transversely draining streams from normal stream segments:

1. Transversely draining streams flow from a region of lower elevation into a region of higher elevation and then back into a region of lower elevation.
2. Contour lines constrict through the breached topographic high.

Until recently, however, manual identification was the only way to recognize these two characteristics on a map (Lee, 2013, 2019, 2021). Here, a method is presented which uses the relatively new technique of relative elevation modelling to digitally filter a given area for potential TDs. The goal of this study was to create a global set of large-scale TDs on streams longer than 200 km, which can then be used to identify areas for future investigation. While not totally eliminating the need for manual verification, the method offers an efficient way to identify potential areas of study, since the existence of TDs may indicate significant past drainage rearrangement.

Currently, relative elevation modelling has been used on very small scales with high resolution digital elevation models (“DEMs”) like Lidar to determine areas of elevation differences in river floodplains (Greco et al., 2008; Labas et al., 2024, Shinn, 2015; Coe & Wolfe, 2016, Olson et al., 2014, Owen and CASLYS Consulting, 2024). Past studies include Wang et al. (1984), who used LANDSAT imagery to estimate a relative digital terrain model in mountainous areas, Poole et al.’s (2002) creation of an algorithm to derive a relative elevation model, and Greco et al. (2008), who described a process to calculate the relative elevation of flood-plain elements to the Nyack flood plain of the Middle Fork Flathead River, MT, USA. Ni et al. (2024) presented a technique for creating a relative elevation model with more than one stream, but their methodology required a medium-low

resolution digital elevation model and was only used on three streams. The process described here, however, allows relative elevation modelling of thousands of streams using any resolution of DEM.

METHODOLOGY FOR TRANSVERSE DRAINAGE IDENTIFICATION

Relative elevation modelling components

Relative elevation models ("REMs") are created by using a line feature, a raster terrain layer, and a Geographic Information System ("GIS") (OpenTopography, 2022). During the process of REM generation, the elevation of the streamline is set to zero, and all the elevation points in the surrounding window are adjusted accordingly. In Global Mapper, the GIS used in this study, the REM is calculated from the difference between the original input terrain and an intermediate raster terrain layer generated based on interpolated Inverse Distance squared Weighted (IDW) elevations pulled from the original terrain nearest to the line feature.

Figure 1A-B is a comparison of a DEM and a REM of the Colorado River (US) using the SRTM Plus V-3 DEM (~30 m resolution, (U.S. Geological Survey, 2014)) and a vector streamline of the Colorado River from the HydroSHEDS project's RiverATLAS database (Linke et al., 2019, available at https://www.hydrosheds.org/hydroatlas). Elevations below 0 in both figures are shown in blue. In Figure 1A, zero elevation is equivalent to sea level, and areas below sea level are limited to the Salton Sea region and the Gulf of California. Figure 1B is the same area with all elevations adjusted by the REM to be relative to the Colorado River. The blue areas near the head of the river indicate that the Colorado watershed is relatively higher than the Great Salt Lake and Snake River basin to the west, and to other basins in Wyoming and Colorado to the north. Further downstream, other areas relatively lower than the river include the lower Gila River and an expanded area around the Salton Sea. Figure 1C is a combined profile of the Colorado River from the SRTM DEM (blue) and from the REM (red), illustrating how the REM removes the decreasing elevation trend of the streamline. The spikes in the profiles result from mismatches between the SRTM Plus V3 elevation pixels and the RiverATLAS streamline vectors, which were created on a DEM that had been upscaled from SRTM to a 3 sec DEM with ~500 m resolution (https://www.hydrosheds.org/hydrosheds-core-downloads, accessed December 15, 2025).

The distinctive utility of REMs for transverse drainage identification is that a swath profile along the river at a given distance around the stream channel would capture the average elevations within that range, allowing identification of the high grounds relative to the river (Fig. 1D-E).

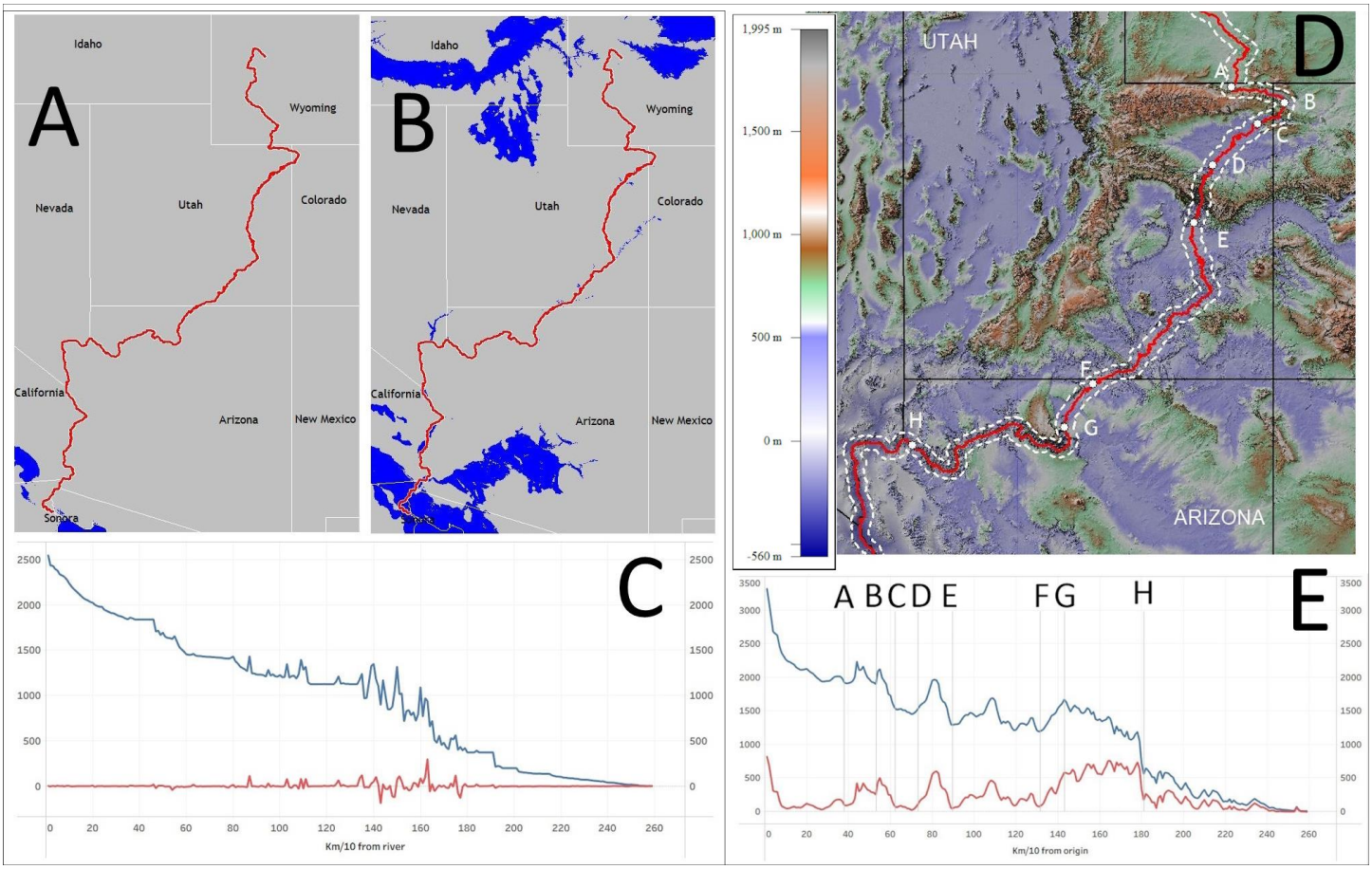


Figure 1. (A) SRTM digital elevation model (DEM) around the Colorado River (US) with zero elevation equal to sea level. Areas below sea level shown in blue. Length units in km, elevations in meters. (B) Relative elevation model (REM) of the same area with all elevations adjusted to be relative to the Colorado River, with areas below the Colorado River shown in blue. (C) Combined profile of the Colorado River from the SRTM DEM (top, in blue) and from the REM (below, in red). Spikes in profiles result from imperfect match between the river's line vector and the underlying topography and result in the deviations in Figure 3 of proxy values from the actual values. (D) Colorado River in red, 20 km wide swath profile corridor indicated by dashed white lines. A: Flaming Gorge entrance, B: Lodore Canyon entrance, C: Split Canyon, D: entrance of Desolation Canyon through the Tavaputs Plateau, E: Desolation Canyon exit, F: Glen Canyon Dam, G: entrance of Grand Canyon through Kaibab Plateau, H: Grand Wash. The color shading for this map is a dynamic shader that changes to match the available elevations in the GIS window, allowing for better visualization of contrasts in relief at different elevation scales. (E) DEM and REM 20 km wide swath profiles of average elevations around the Colorado River. DEM profile in blue, REM profile in red. Letters refer to locations in Figure 1D.

The most straightforward way to replicate a swath profile corridor in a GIS for the purpose of TD identification would be to create a buffer around the streamline at the desired distance, then divide it into segments and compare the segments to each other. However, while it's possible to create a buffer around a stream in Global Mapper equivalent to a swath profile corridor, it's not possible to divide it into equal segments. The

technique presented here creates a proxy for a swath profile by creating evenly spaced points along the stream and then generating overlapping circular buffer areas around the points.

Figure 2A shows the section of the Colorado River through the Kaibab Plateau and the Grand Canyon, with points spaced 10 km apart, and Figure 2B shows circular point buffers (CPBs) of 20 km diameter generated from those points. Figure 2C shows the close overlap of the CPBs with a 20 km wide buffer (red lines) around the river.

Once CPBs are created, the GIS can calculate their elevation and slope statistics, including average elevation and average slope percent. On an unmodified DEM, the average elevation of the CPB would be relative to sea level, but on a REM, it would be relative to the river. Plotting the average elevations of the REM CPBs on a graph by distance from the origins gives the ability to identify the high grounds, i.e., the TDs, through which the river flows. Because the buffers overlap each other by about 50%, they allow for more complete coverage when graphing changes in attributes along the stream. The utility of this system is that it can be scaled up or down by varying the point spacing and the buffer diameter, depending on the resolution desired for the analysis.

One problem with relative elevation modelling as a GIS technique is that it can only process one streamline at a time. The methodology described here, however, creates a proxy for the REM average elevation of a CPB by subtracting the DEM elevation of its center point from the DEM average elevation of the CPB. For example, if a point has an elevation of 66 m and the CPB generated from the point has an average elevation of 140 m, the average CPB elevation minus the origin point's elevation is 74 m.

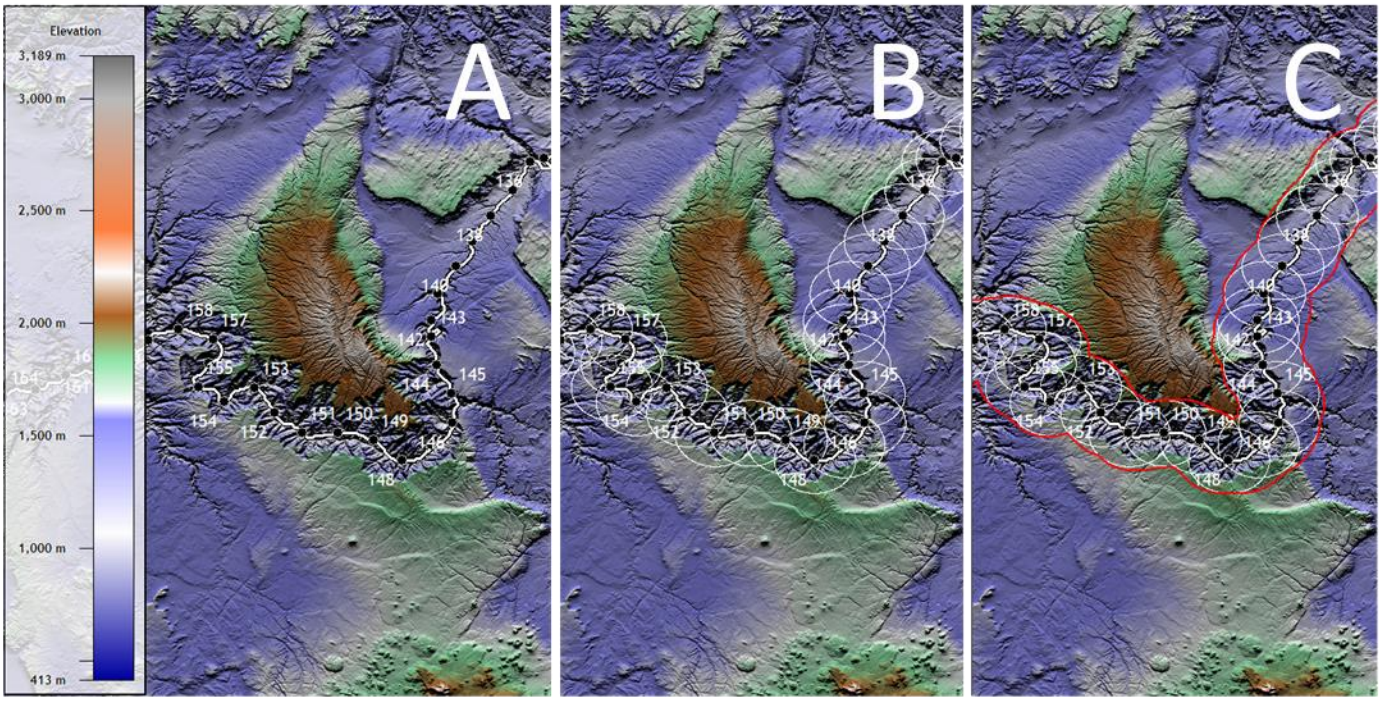
The result is a proxy for the relative average elevation of the CPB that proves to be substantially equivalent to the value calculated from a REM. Figure 2D plots the actual REM average elevations of the Colorado River CPBs against the REM proxies derived by subtracting the SRTM point elevations from the SRTM average elevations of the CPB. In Figure 2D, the circles represent CPB REM proxy values within one standard deviation of the mean, and the X's represent values outside one standard deviation. All the values outside one standard deviation result from midpoints which imperfectly match the underlying topography because of the DEM upscaling that was used to create the original HydroSHEDS stream vectors. These mismatched points result in deviations of proxy values from the actual values, but even so, the combined r^2 value for the plot is .95 with a P value < .0001. When the points outside the standard deviation are removed (n=35, 14% of total), the r^2 becomes .99. These results give confidence that:

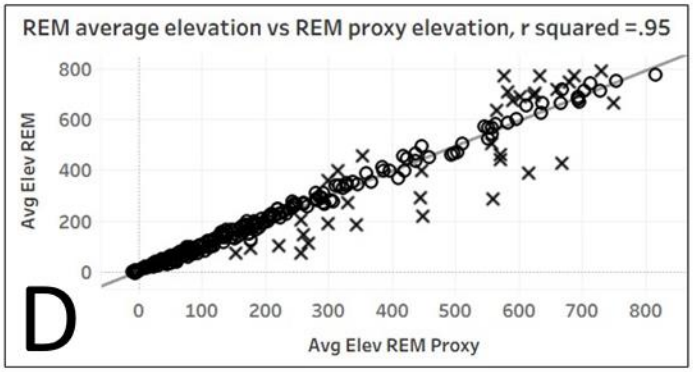
1. The deviations are not random, but result from the “noise” created by the difference between the HydroSHEDs DEM from which the stream vectors were produced and the SRTM DEM from which the REM was generated.
2. The value derived from subtracting the DEM elevation of the center point from the DEM average elevation of the CPB is a reasonable proxy for the REM average elevation of the CPB.

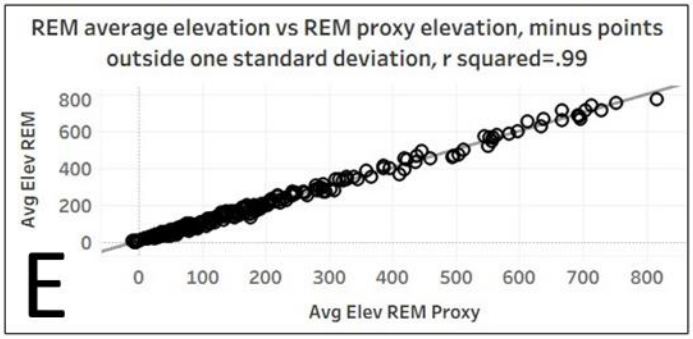
   The ability to create an easily derived proxy for REM average elevation allows the processing of thousands of km of streamlines without much computational effort.

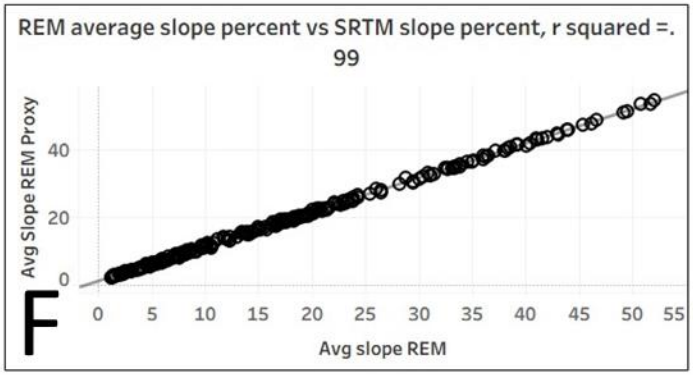
Figure 2C shows that, for the CPB statistic of average hillslope percent, there is very little difference between the REM vs. DEM values. This occurs because slope is affected only slightly by the elevation adjustments of a REM generation, so no proxy was necessary for the average hillslope percent of CPBs.

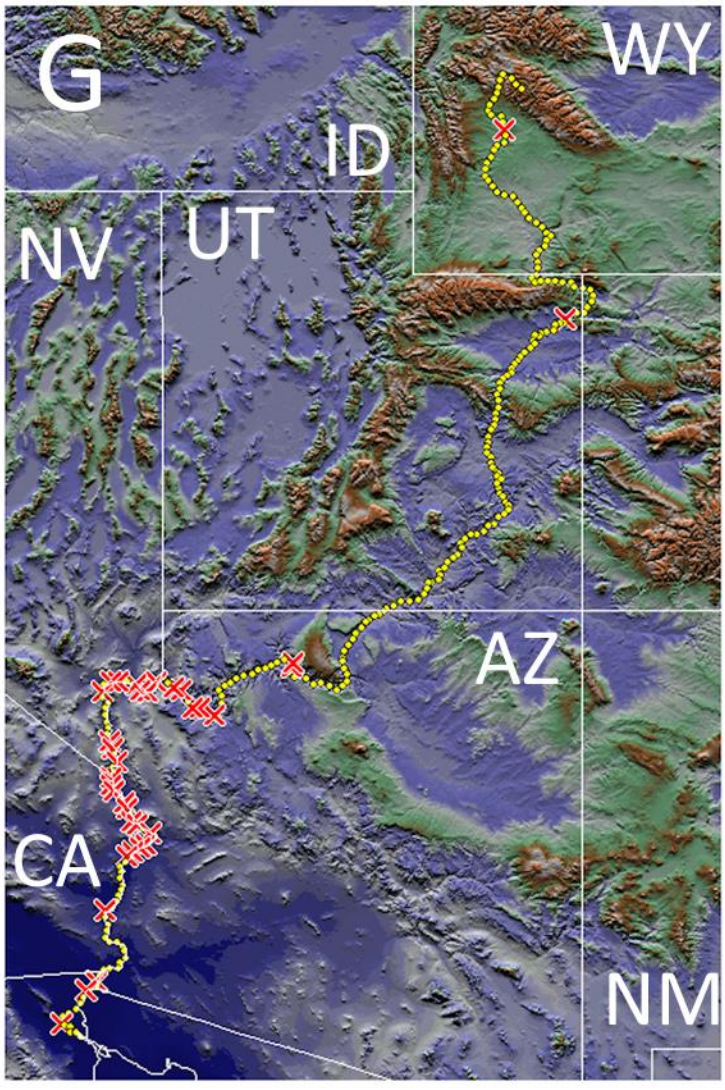
Figure 2. (A) (Points spaced 10 km apart along the Grand Canyon of the Colorado River through the Kaibab Plateau. (B) Circular point buffers (CPBs) generated from the points. (C) 20 km buffer (red lines) around the river, showing close size correspondence of CPBs to buffer. (D) Y-axis is CPB average elevation from the REM of all the points along the Colorado River in Fig. 2H, X-axis is average elevation from the REM proxy (CPB average elevation from the DEM minus elevation of the midpoint). X’s on plot represent values greater or less than one standard deviation from the mean. (E) Figure 2D with values outside one standard deviation removed, changing the r^2 from .95 to .99. (F) REM average hillslope angle percent of CPBs plotted against SRTM average hillslope percent of CPBs. (H) Locations of points in 2(D-F) along the Colorado River. Yellow dots are the locations of the REM proxy average elevation values within one standard deviation of the trend line, X’s are points greater or less than one standard deviation.


Elevation
3,189 m
3,000 m
2,500 m
2,000 m
1,500 m
1,000 m
413 m
A
B
C


REM average elevation vs REM proxy elevation, r squared =.95
Avg Elev REM
Avg Elev REM Proxy
D


REM average elevation vs REM proxy elevation, minus points outside one standard deviation, r squared=.99
Avg Elev REM
Avg Elev REM Proxy
E


REM average slope percent vs SRTM slope percent, r squared =.99
Avg Slope REM Proxy
Avg slope REM
F


G
ID
WY
NV
UT
AZ
CA
NM

Study components

The purpose of the analysis was to identify large scale transverse drainages for further investigation. The components of the TD identification process included:

1. Three DEMs allowing for global coverage:
    - To increase the correspondence of CPB slope statistics to the RiverATLAS streamlines, the conditioned DEM from which the streamlines were generated was used for all streams within its areal extent of 60°N-56°S (https://www.hydrosheds.org/hydrosheds-core-downloads, accessed December 12, 2025).
    - MERIT DEM with 3 arc-seconds spacing and ~90 m resolution (Yamazaki et al., 2019), was used in the areas where the HydroSHEDS DEMs were not available.
    - For a few points outside of either of these DEM extents, the ETOPO 22 DEM was used (15 arc-seconds,~ 450 meters) (National Centers for Environmental Information, 2022).
2. Streamline shapefiles were taken from HydroSHEDS project's RiverATLAS database.
3. Points spaced 10 km along the streams and circular point buffer areas of 20 km diameter created around the points,
4. Global Mapper was used for the GIS, and Excel for analyzing CPB attributes.

One issue with RiverATLAS is that the line vectors are only available as stream segments, but the study methodology requires a file of streams that extend from source to sink without interruption. However, each RiverATLAS segment contains an attribute of classic stream order, where order 1 is the main stem river from source to sink, order 2 represents all tributaries flowing into a 1st order river, etc. Merging all the segments by stream order in the GIS allows the creation of single streams. The lower limit on stream length was set at 200 km to ensure that at least 20 CPBs would be created on the streamline. In total, the large-scale study generated 265,185 CPBs on 6557 streams with a combined length of 2,618,692 km.

Every stream and point in the dataset were given database index numbers. RiverATLAS assigns an 8-digit number to trunk streams in its dataset, so the streams in this study were assigned a stream index number composed of the RiverATLAS trunk stream number and the numerical order of the stream's length in the watershed. For example, the Colorado River is a trunk stream and its RiverATLAS index number is 70765249, so its study index number is 70765249 – 1. The study index number of the Gila River, the next longest tributary of the Colorado, was 70765249 – 2, the third longest stream was 70765249 – 3, etc.

Because the classical ordering system used by RiverATLAS considers a trunk stream to originate with the stream segment that is farthest upstream from the ocean outlet, some of the trunk streams look different

than conventional river systems. For example, in the Colorado River watershed, the head of the Green River is the farthest stream segment from the Gulf of California, so a combined Green-Colorado River became the trunk stream in the RiverATLAS dataset, while the stretch of river normally considered to be the upper Colorado River was treated as a tributary of the trunk stream.

The streams were divided into 10 km segments and were labeled numerically in order downstream from the stream origin. Midpoints were generated for each segment, and CPBs created around each point with a 10 km radius in order to create overlap. Every point and CPB received the same index number as the segment from which it was generated. Additionally, each 10 km segment was divided in half, and CPBs were generated from the midpoints of each half segment with a radius of 5 km. This was done to capture smaller scale TDs that might escape the larger resolution of the 20 km diameter CPBs.

Lithologic attributes were joined to the CPBs from the GLIM database (Hartman & Moosdorf, 2012), hydrologic attributes such as long-term average discharge, stream size and stream power from the HydroSHEDS databases, and tectonic settings from the Bally (2007) Tectonic Map of the World GIS dataset. Streams located within or originating within the last glacial maximum and the MI6 glacial boundaries of Batchelor et al. (2019) and Ehlers et al. (2011), were given an attribute of "GLACIALLY_INFLUENCED," and this attribute was passed onto any TDs located on the stream (GIS files for Ehlers et al. (2011) available at https://www.arcgis.com/home/item.html?id=046cde34ce804141a8d5303656e74f44 (Hall, 2022); GIS files for Batchelor et al., (2019) available at https://osf.io/7jen3/overview). The HydroBASINS L03 global basin dataset (Lehner & Grill, 2013), which contains 288 basins and coastal drainage areas and which correlates to the RiverATLAS streams, was used to group the streams by basin.

Table I. Example of the database numbering system for the study vector features using a point generated from the tenth segment downstream from the origin of the Colorado River.

Shapefile type	Stream index number from RiverATLAS	Stream rank in watershed by length	Numeric order of stream segment from stream origin	Study Index number
Stream	70765249	1	N/A	70765249 - 1
Point: Segment midpoint	70765249	1	10	70765249 - 1 - 10
Area: Circular point buffer (CPB)	70765249	1	10	70765249 - 1 - 10

Once points and CPBs were created, Global Mapper was used to calculate their elevation and slope statistics. In this study, the three CPB attributes for TD identification were:

1. The proxy for REM average elevation, as described above and in Figure 3, labeled “REM-AE.”
2. The mode of elevation of the CPB minus the point elevation, as an additional diagnostic tool for CPBs with lower relief, labeled “REM-ME.”
3. The DEM average slope percent (“ASP”), which tended to increase as stream channels narrowed through TDs. As noted above, there is no significant difference in slope values between the REM and the DEM, so no proxy was needed.

The REM-AE minimum for the dataset was set at >100 m, the REM-ME minimum at >50 m, and the ASP minimum at >12%, based on comparison with the attributes of CPBs through well-known TDs such as the Grand Canyon of Arizona (US).

All the CPBs were imported into Excel, and spreadsheet functions were used to identify possible transverse characteristics, including calculating moving averages for both REM-AE and REM-ME to smooth out the signal. Three iterations were carried out to identify individual CPBs as either “Positive” for possible investigation or “Negative” because none of the filtering thresholds were crossed:

The first iteration was applied to the 10 km CPBs. If any of the following applied, the CPB was labeled “Positive”:

- The moving average or original value of the REM-AE exceeded 100 m.
- The moving average or the original value of the REM-ME exceeded 50 m.
- The ASP exceeded 12%.

For the second iteration, the three minimum thresholds were applied to the 5 km half-segment CPBs without calculating a moving average. If a half segment received a positive value, that was applied to the 10 km segment from which it was derived.

In the third iteration, if a 10km CPB was identified as “Negative” but was located adjacent to a TD labeled “Positive”, it was re-classified as a positive because the 50% overlap of buffers meant that its midpoint was located within the buffer of a possible TD.

Excel IF functions were then used to combine consecutive 10 km CBPs into individual stream reaches based on their possible TD classification, and each reach was given a unique reach index number.

Reaches identified as possible TDs were then manually inspected in the GIS and in Google Earth to determine whether they met the two diagnostic criteria for TDs:

- Streamflow from a region of lower relative elevation into a high ground.
- Constriction of contour lines through the high ground.

In addition to contour constriction, indicators supporting transverse identification included the following:

- Two or more tributaries joining just upstream of a TD.

- Marked change in channel morphology, such as straight to sinuous.
- Abrupt change in channel bearing,
- Existence of a dam on the possible TD.
- Existence of another verified TD upstream or downstream.

Possible TD reaches that met the criteria for transversity were assigned the value of "True" for a new attribute labeled "VISUAL." All false positives received one of the following values:

- X: Apparent structural breaching without upstream contour constriction.
- U: Apparent upstream contour constriction without a breached structure.
- W: A "wall effect," where streams migrating across a level valley floor appeared to increase in relative average elevation as they approached the valley wall.
- N: A narrowing effect triggering a value above the minimum for one of the three CPB slope statistic attributes. This was the most common cause of false positive identification, and resulted from one of the following circumstances:
    - Channel slopes approaching each other as channel width varied.
    - Deeply incised channels in plateaus or hillslopes.
    - Stream reaches flowing down knickpoints at the edges of level plateaus, causing the relative average elevation of CPBs to increase as the stream descended.

Because of the relative coarseness of the filtering algorithm, not all pour points into the TD were located on the first segment of a visually verified TD; however, all CPBs upstream of the pour points were included as part of the TD on the basis that their steep slopes and high relative elevations should have some genetic connection to its origin. On average, pour points were located about five segments from the origin.

The process of visual verification revealed a few false negatives, where CPBs were clearly TDs but had slope statistics too low to trigger a possible TD identification. These were usually located very near an actual verified TD.

All verified transversely-influenced reaches were given a geographic label derived from the combination of the stream name and the main trunk stream of the watershed. For example, the TD reach of the Colorado River through the Grand Canyon is labeled "Green-Colorado – 133" because the river name is "Green-Colorado" and the first point on the reach is segment 133. Names of rivers were derived from several sources, including Google Earth, OpenTopoMap, and geographic locator websites such as Mapcarta.com. Additionally, the HydroDAMS database was used to identify any dams in the database located on the TDs.

Verification of TDs was most difficult in areas of extensive valley glaciation in the Arctic regions of Europe, North America and Asia, and in Patagonia and the New Zealand Alps. In these regions, pre-glacial stream networks have been deranged by fluvial erosion in meltwater channels, creating breached divides and through valleys (Bloom, 1998; Brardinoni & Hassan, 2006). TD identification was still possible, but required more reliance on additional indicators such as dams or changes in channel morphology and bearing.

Artificial intelligence and terrain processing

After the visual verification was completed, three attempts were made to see if artificial intelligence (AI) could be used to replicate and automate the verification process.

Google's Gemini was used first because it is the only AI to have direct, bi-directional access to Google Maps and Google Scholar. A file of latitudes and longitudes for stream segment midpoints was fed into the AI and it was prompted to identify any transverse drainages. Unfortunately, it got the river name or flow direction wrong so often that it was unreliable, especially considering the number of TDs in this study. When queried why it was so bad at geographic identification, it responded that it was trained to regionally approximate when it couldn't pinpoint a location. Additionally, AI's are programmed to preference production of answers even when they don't necessarily know whether the answer is correct.

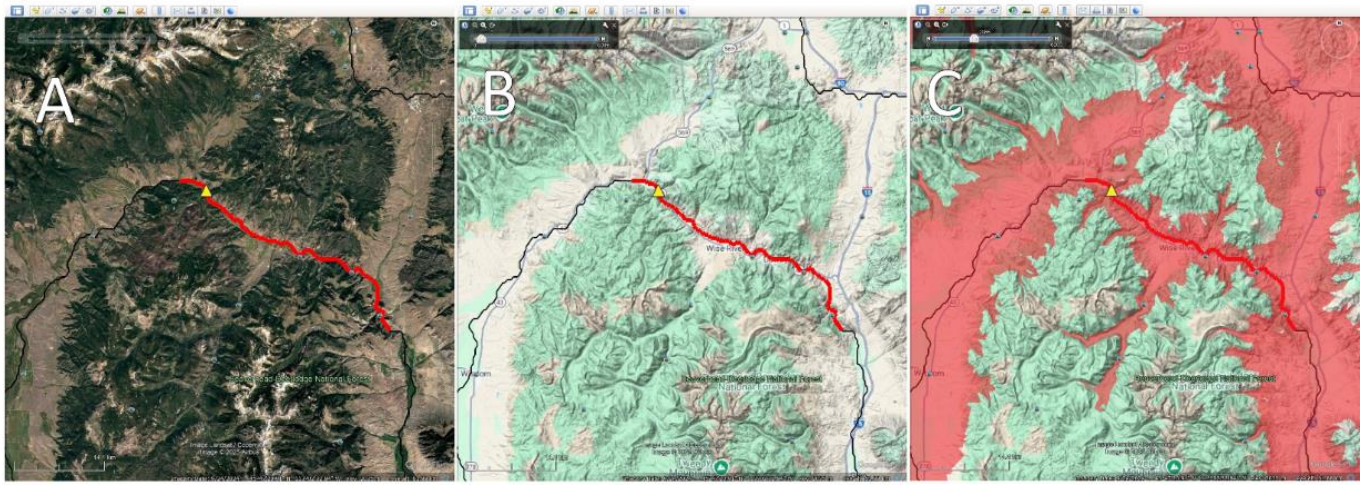
In 2026, a new web-only Google Earth AI was offered for Gemini Pro subscribers called "Ask Google Earth." To see if it could be used to automate TD identification, the AI was queried to see if all the rivers in the study could be uploaded as KMZ files and all transverse drainages located along the rivers. Unfortunately, Ask Google Earth lacks 3D terrain processing and is currently limited to 2D vector math (like finding intersections, calculating areas, or measuring distances between standard points and polygons). It does not have direct access to the 3D topographical data or elevation profiles required to compute where river paths contradict the surrounding terrain gradients. When queried about water gaps along the Colorado River (US), it was able to give locations but only because it could search published research reports to find locations. Unreported TDs are not identifiable. The solution suggested by Ask Google Earth was to create a KMZ of rivers and manually inspect them in a GIS or in Google Earth--the very methodology used in this study!

The third attempt was with Google Earth Engine (GEE), a Google Cloud product for geospatial analysis at scale, which combines a multi-petabyte catalog of satellite imagery and geospatial datasets with planetary-scale computation to accelerate environmental research and applications (Gorelick et al., 2017). As a test for accuracy, all potential TD stream reaches were fed into GEE with a script created by Gemini to identify TDs that met the TD criteria of upstream contour constriction (See Appendix B for complete description). The process, however, missed 40% of verified TDs and misidentifed another 589 as actual TDs when they were not. In the end, visual inspection, though time-consuming, was the simplest and most efficient way to verify a TD.

All the visually verified TDs are available for viewing online at watergaps.com and are available as geopackage files at https://doi.org/10.5281/zenodo.21988478 or upon emailed request as Excel tables, shapefiles and Google Earth KMZ files. The Google Earth KMZ viewing experience is greatly enhanced by downloading the Google Maps terrain view overlay for Google Earth, available at https://ge-map-overlays.appspot.com/google-maps/terrain (Fig. 3B).

Included with the KMZ files is a Sea Level Rise ("SLR") slider, which can be manipulated in Google Earth to simulate rising sea level by moving the historical time slider at the top left of the Google Earth window. Using the SLR slider allows clearer identification of the lower elevations upstream of the TD and emphasizes the constriction of contours through the high ground (Figure 3).

Figure 3. (A) Google Earth view of the TD of the Big Hole River through the Pioneer Mountains of Montana, US. Yellow triangle indicates pour point into the TD. (B) Same view with Google Maps Terrain overlay enabled. (C) Google Maps Terrain overlay with Sea Level Rise slider set to approximately 2000 m ASL, delineating more clearly the lower elevation terrain upstream of the TD.



RESULTS

A transverse drainage is defined in this methodology as a stream reach consisting of one or more transverse segments connected by intermediate consequent reaches. These were identified as possible TDs through the filtering and aggregation process, and were visually verified to flow from regions of lower relative elevation into regions of higher elevation, with constriction of contour lines through the high grounds.

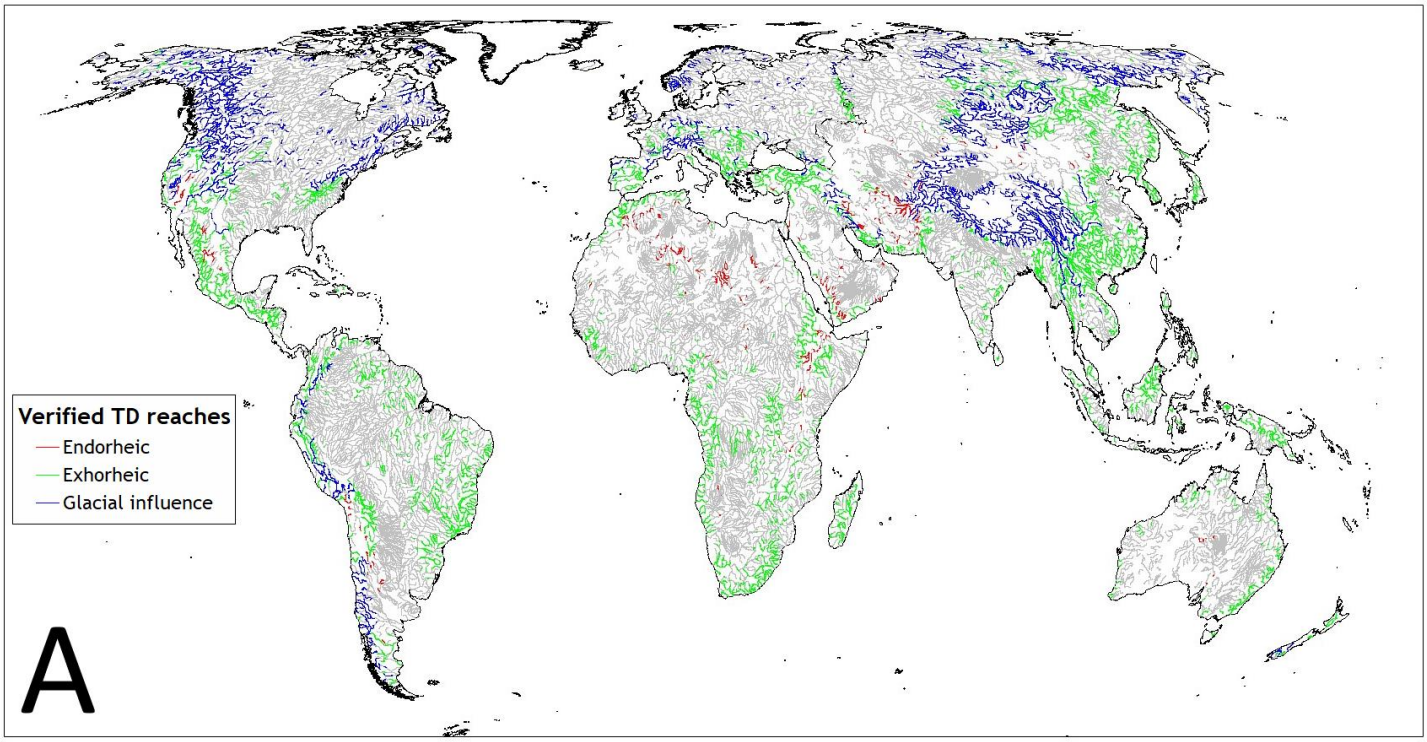
Global transverse drainage distribution and comparison with non-transverse reaches.

The methodology resulted in 3953 visually verified TD reaches on 2921 streams located in 190 HydroSHEDS basins (Fig 4A-B). The results are summarized in Table II. Verified TD reaches comprised three-fourths of the total potential TD stream length, and 25% of the total stream length in the study. Figures 4A-B are maps of all visually verified TDs, and Figures 5-6 are charts of the TD attributes.

Table II. Percentage of TD reaches and TD reach length in dataset.

Potential TD	Number of stream reaches	Length	% of total stream length	
Not TD	10,227	1,752,714		67%
Possible TD			**% possible TD length**	
No	3,341	208,451	24%	8%
Yes	3,953	657,527	76%	25%
Possible TD subtotal	7,294	865,978		
TOTAL	11,746	2,618,692		100%

Figure 4A-B. (A) All visually verified TDs. Global river dataset in grey, glacially influenced TDs in blue, unglaciated exorheic TDs in green, unglaciated endorheic TDs in red. (B) Watershed basins shaded by TD density.



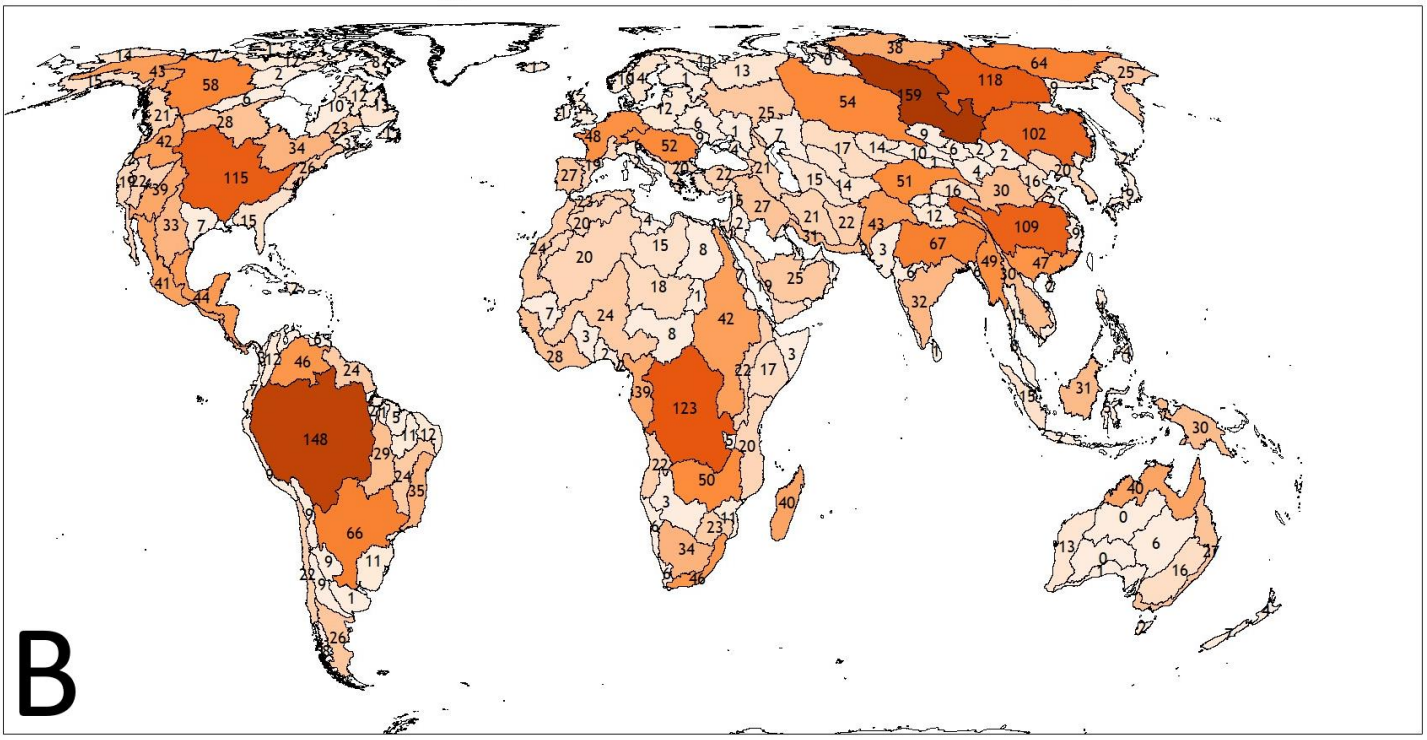
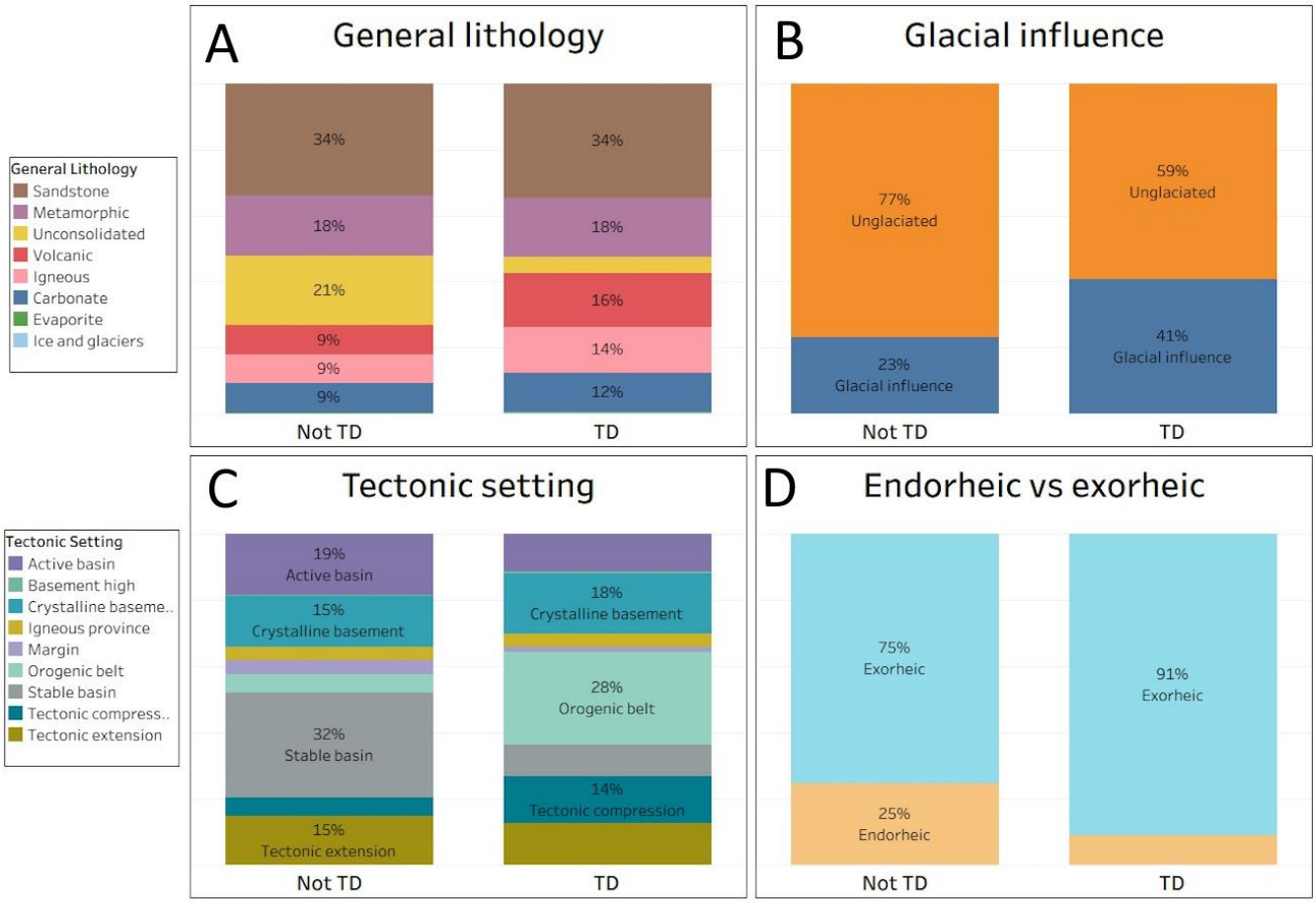
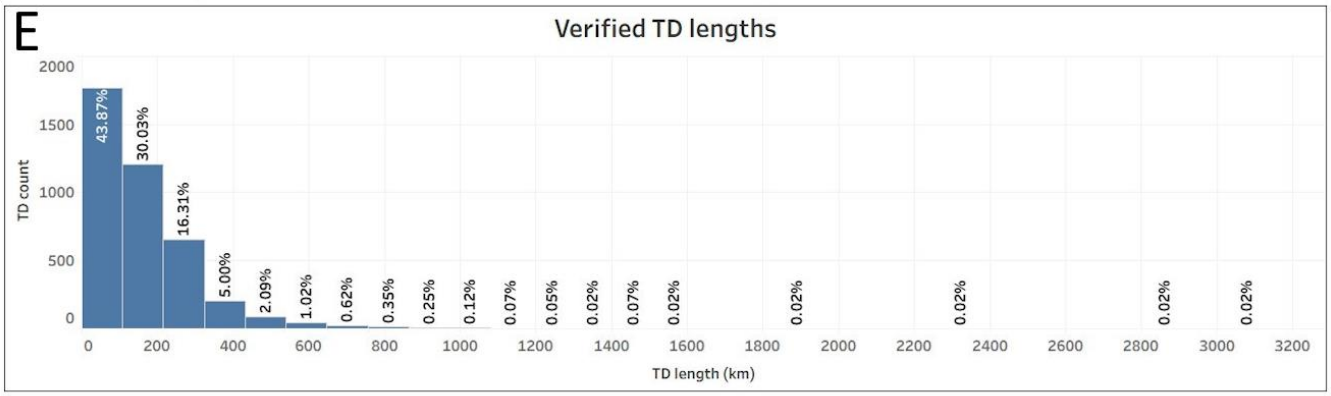


Figure 5A-F. (A-D) Comparison of TD vs non-TD attributes: A) Lithology of the maximum elevation of the reach; B) Distribution on glacially influenced streams; C) Tectonic setting; D) Percentage of exorheic vs endorheic streams. (E) Distribution of TD lengths. (F) Distribution of stream size and stream power at TD pour points.





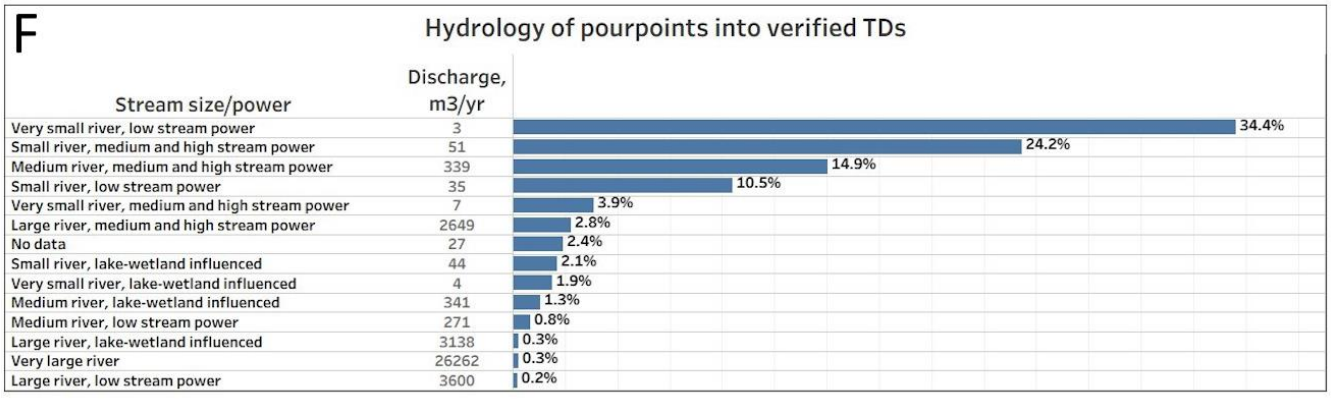


Figure 6A-E. Average maximum depth of verified TD reaches by attribute. Clockwise from top left: Lithology, Glacial influence, Stream hydrology at pour points, Endorheic vs exorheic, Tectonic setting.

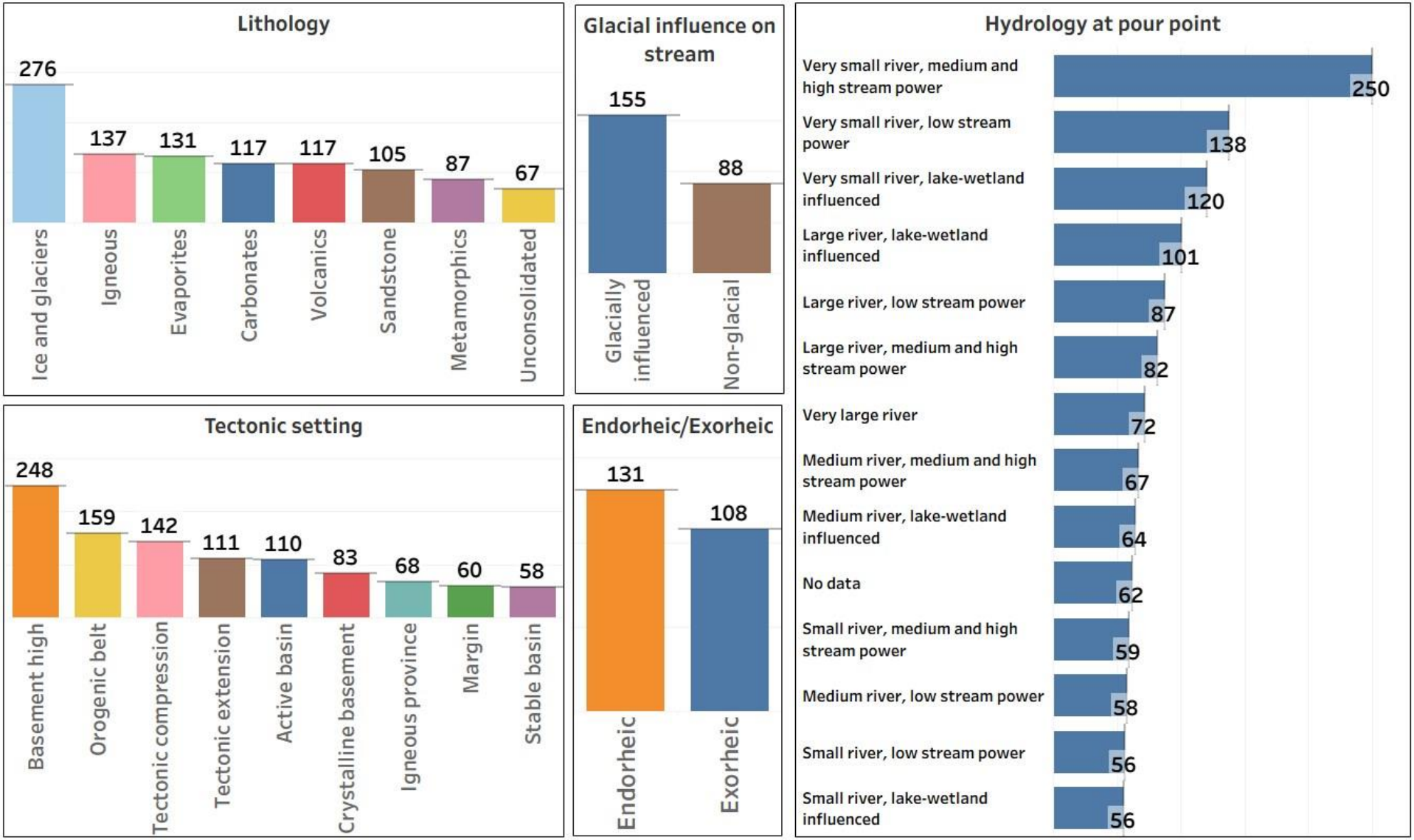


Figure 5 (A-D) compares verified transverse reaches to non-transverse reaches for lithology, glacial influence, tectonic setting, and endorheism. Because of a possible relationship to the potential origin of a TD, the lithology of the highest elevation in each reach was compared between transverse and non-transverse reaches. While sandstones form the largest percentage of the high point lithologies of both types, unconsolidated sediments form the high ground in 21% of non-transverse reaches but only 5% of transverse reaches. Compared to non-transverse reaches, verified TDs have a higher percentage of glacial influence and exorheism, and their most common tectonic setting is orogenic belts, while stable cratons form the most common setting for non-TD reaches.

Characteristics of transverse reaches

Figures 5-6 suggest that the most representative TD in this study will be less than 100 km long and located in an unglaciated orogenic belt with sandstone lithology, and at the pour point will be a very small river with low stream power and discharge. The deepest TDs, however, are found in TDs originating on very small rivers in glaciated areas or on basement highs. Interestingly, TDs in endorheic areas are significantly higher in general than exorheic streams.

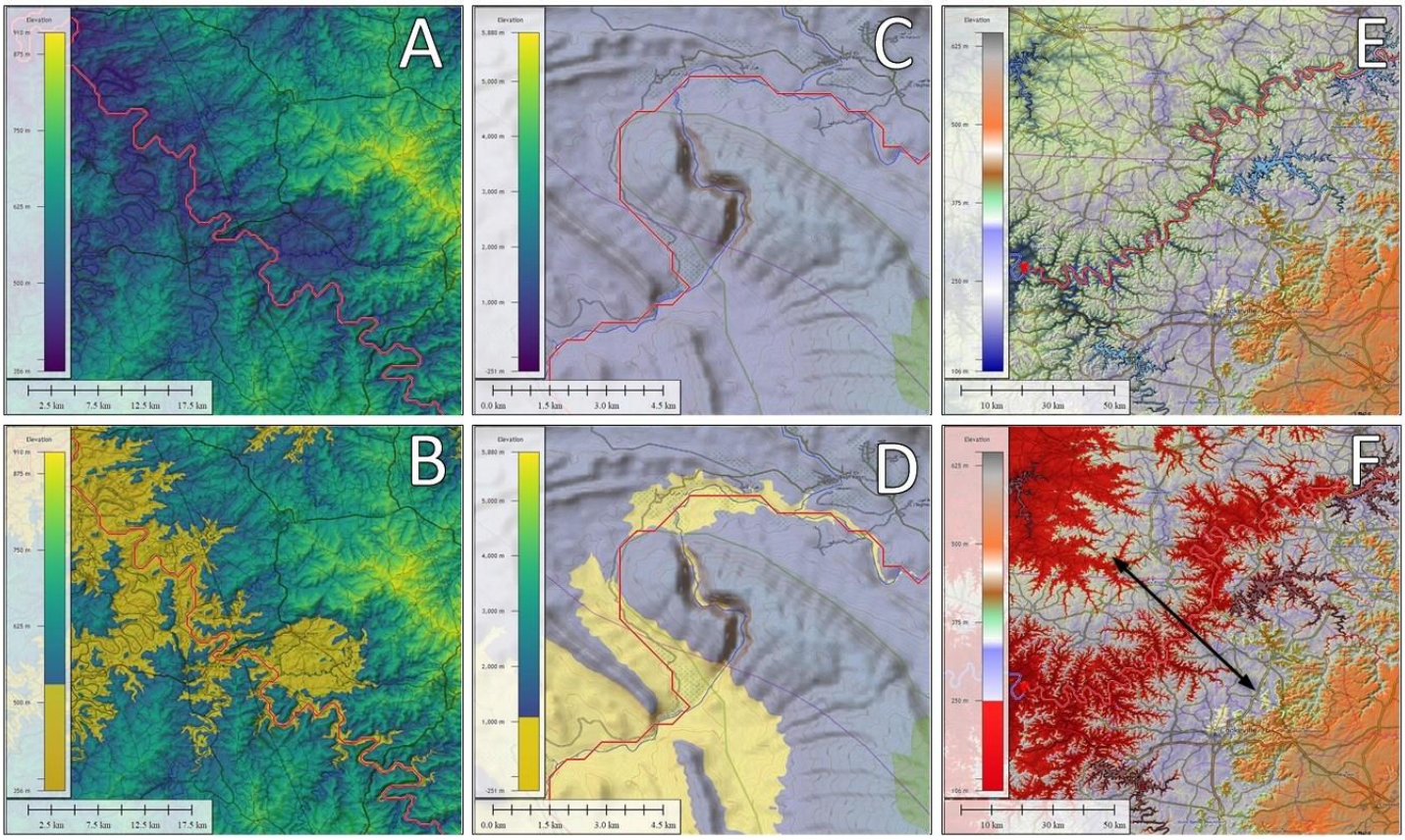
Dams in the HydroDAMS database were located on seventeen percent of the TDs. As would be expected, the majority of TDs are located in mountain belts, including the North and South American Cordilleras, the trans-Alpine belts of Europe and Asia, and the Asian Himalayas. However, the largest concentration of transverse drainages is found in Siberian watersheds with streams flowing into the Arctic Ocean (Fig. 4B). These are almost certainly controlled by sub-glacial flooding and glacial outburst floods (Herget, 2005; Batbaatar & Gillespie, 2015; Arzhannikov et al., 2017; Margold et al., 2018), though there is a question of how much of the drainage direction was influenced by preglacial fluvial systems (Bloom, 1998; Lajeunesse, 2014).

One interesting finding was the prevalence of TDs along the margins of cratonic shields (Fig. 4A). For example, along the southern coast of Africa from the Niger River in the west to the Bay of Maputo in the east, all but four of the streams in the database had transverse reaches. In South America, every eastward flowing database stream on the eastern coast from the mouth of the Rio Curimatau to the Paraibo do Sul River had transverse reaches. All the database rivers draining from the central Alaskan-Canadian plateau along the Pacific Northwest had transverse stretches, from the Copper River to the mouth of the Fraser River at the meeting of the Straits of Georgia and Juan de Fuca.

While many spectacular TDs in the study are well-known, such as the Grand Canyon, the Columbia River through the Cascade Mountains, and the many TDs through the Cape Fold mountains of South Africa, there are many impressive TDs that are less well-known. Figure 7A-D show two unusual TDs picked up by the methodology, on the Rio Chopim in South America and the Qara Aghaj river in Iran. In Figure 7A-B, the Rio Chopim flows consequent to structure, then flows into a meteor bleme and out through a ridge on the other side. In Figure 7C-D, the Qara Aghaj flows through the nose of an anticline so narrow that the HydroSHEDS DEM could not pick it up, so the TD is shown flowing around the anticline instead of through it.

Surprisingly, the methodology was able to pick up many subtle features as well. For example, in North America, the methodology picked up the crossing of the Cumberland River over the Cincinnati Arch (Fig. 7E-F), which is not very apparent in a standard topographic map but shows up well when elevations below 250 m are shaded.

Figure 7A-F. TDs (red lines) on the Rio Chopim (Brazil), Qara Aghaj (Iran) and Cumberland River (Kentucky, United States). (A) Rio Chopim flowing northwest to its junction with the Iguazu River. (B) Rio Chopim TD, elevations below 530 m shaded yellow, showing the path of the river flowing into a meteor bleme and then out across a ridge. (C) A portion of the TD of the Qarah Aghaj. The actual river flows through the narrow canyon in the anticline nose, but the HydroSHEDS stream in red passes around the nose because the channel was too narrow to be captured by the resolution of the DEM from which the streamline was generated. (D) Qara Aghaj, elevations below 1080 m shaded yellow, illustrating contour constriction upstream of the gap. (E) Cumberland River flowing from Kentucky into Tennessee. (F) Cumberland River, elevations below 250 m shaded red, showing the river breaching the Cinncinnati Arch (arrow).



One of the most useful applications of the methodology is the ability to identify and analyze TDs in remote and hard to access locations. The example of the Congo River watershed will be used to illustrate how identified TDs can be integrated with theories of TD formation.

TRANSVERSE DRAINAGE FORMATION THEORIES

Currently, there are four major theories for the formation of transverse drainages: overflow/spillover, antecedence, superimposition, and stream capture/piracy (Bishop, 1995; Burbank et al., 1996; Clark, 1989; Douglass et al., 2009; Douglass and Schmeeckle, 2007; Morisawa, 1989; Twidale, 2004).

Overflow refers to the phenomenon of impounded water overtopping a barrier, and can range in scale from small basins to paleolakes (Hilgendorf et al., 2020, He et al., 2026). Antecedent TDs are hypothesized to have formed when a pre-existing drainage preserved its original course during the uplift of buried resistant layers (Bishop, 1995; Burbank et al., 1996; Twidale, 2004). Superimposition occurs when a pre-existing stream network maintains its original channel and direction of flow as it erodes away a covermass and cuts down through buried ridges (Douglass & Schmeeckle, 2007; Larson et al., 2017). The primary difference between antecedence and superimposition is that antecedent streams are older than the high grounds through which they flow, while superimposed streams are younger, having eroded a covermass and incised into buried pre-existing high grounds. In stream capture, also known as stream piracy, streams erode headwards or laterally through divides to capture the drainages of other streams (Bishop, 1995; Douglass and Schmeeckle, 2007; Hilgendorf et al., 2020).

Bishop (1995) further classified stream capture in terms of either "top-down" or "bottom-up" drainage rearrangement. In top-down processes, a stream "pushes" itself into another catchment, which generally involves divide breaching by the diverted channel as a result of channel migration, tectonism or catastrophic flows (Bishop, 1995). The primary requirements are a low relief interfluve and a steeper gradient for the capturing stream (Bracciali et al., 2015; Larson et al., 2017). Mechanisms include downstream channel aggradation, stream lateral erosion removing the topographic barrier, also known as drainage diversion, and sapping undermining the interfluve (Douglass and Schmeeckle, 2007; Larson et al., 2017). Hilgendorf et al. (2020) argued that top-down drainage rearrangements should properly be regarded as forms of overflow or spillover, referring to them as “aggradational spillover.” The main difference between aggradational spillover and normal basin overflow is that the sediment mobilized during basin overflow comes from within the upstream basins, whereas the flow of sediment from an aggradational spillover switches from one stream channel to another without significant long term storage of sediment (Hilgendorf et al., 2020).

In bottom-up processes, a river actively intercepts and abstracts an adjacent system, most commonly by headward erosion through a divide (Bishop, 1995). Headward erosion mechanisms include mass wasting, in situ weathering, rain splash, sheetwash, knickpoint recession, groundwater sapping and spring sapping of amphitheater-headed valleys, often related to zones of weakness along the divide (Pederson, 2001; Hill et al., 2008; Hilgendorf et al., 2020). Hilgendorf et al. (2020) pointed out that the term “headward erosion” has also been used to describe the propagation of knickpoints up a pre-existing channel, which is not a form of stream capture. They proposed that the term "drainage-head erosion" should be used instead, which is how bottom-up processes of stream capture will be referred to in the following study.

Antecedence, stream capture and superposition have all been proposed as theories for the origin of transverse drainage on the Congo River in Africa. However, an analysis of the database TDs suggests that overflow is a more plausible origin.

TRANSVERSE REACHES IN THE CONGO RIVER BASIN

Overview

The Congo River basin is one of the world’s most remarkable watersheds in terms of its biodiversity, hydrology, and geology. Its unique location straddling the equator and its large size and semi-circular shape allow the Congo to maintain a near constant flow year-round, making it Africa’s largest river and the world’s second largest by volume, only surpassed by the Amazon (Flügel, 2014, 2015). The approximately 350 km section of the lower Congo contains the world’s deepest section of river channel, the most extensive stretch of rapids and the largest waterfall by volume (Inga Falls) (Oberg et al., 2009). Currents in some parts of the rapids are so strong that genetically different populations of the same fish species have arisen within a few hundreds of meters of each other, unable to meet and breed because of massive currents that prevent movement across the channel (Oberg et al., 2009; Jackson, 2009).

The Congo River harbors the highest fish species richness of any river system on the African continent (Schwarzer et al., 2011), and the dense tropical rain forest of the central basin is the world’s second largest continuous forest, with the highest species richness in Africa (Oberg et al., 2009, Master, 2010, Flügel, 2015). The rain forest is home to large charismatic megafauna such as chimpanzees, lowland gorillas and forest elephants, as well as being the purported home of the reptilian cryptid, Mkole-Mbembe (Master, 2010). A ring structure in the Eastern Kasai may be one of the world’s few tropical impact structures (Monegato et al., 2010).

The high plateaus from which the Congo’s tributaries flow contain some of the world’s richest deposits of stratiform cobalt and copper (Braun et al., 2026). Other mineral resources include gold, alluvial diamonds, and the mineral coltane, a necessary component of modern mobile telecommunication devices. So rich is

the mineral wealth of the Congo basin that René Jules Cornet, whose work in the 1890s uncovered the Congo's immense mineral reserves, dubbed the territory a "veritable geological scandal." (Pham, 2014).

Despite the richness of its natural resources, or perhaps because of it (Pham, 2014), the Democratic Republic of the Congo, which encompasses 62% of the river's watershed, ranks as one of the world's poorest and most politically unstable countries (World Bank Group, 2021). Economic development has been stalled by both natural factors, such as the impassible rapids of the lower Congo, and by political factors such as corruption and civil war. These have prevented significant environmental degradation of the river (Harrison et al., 2016), but have also inhibited the collection of geologic data, especially in the central basin, the "Cuvette Centrale" (Kadima et al., 2011).

The drainage pattern of the Congo in the Cuvette Centrale is unique among African rivers (Pound, et al., 2013). Although the basin is subcircular, there is no convergence of drainage upon a central point. Instead, the tributaries that arise on the southern plateaus flow mostly northward, show little convergence, and join primarily with streams flowing westward from the eastern highlands. Downstream from the junction of the Congo with the Oubangui, the largest of its northern tributaries, drainage is mostly to the southwest.

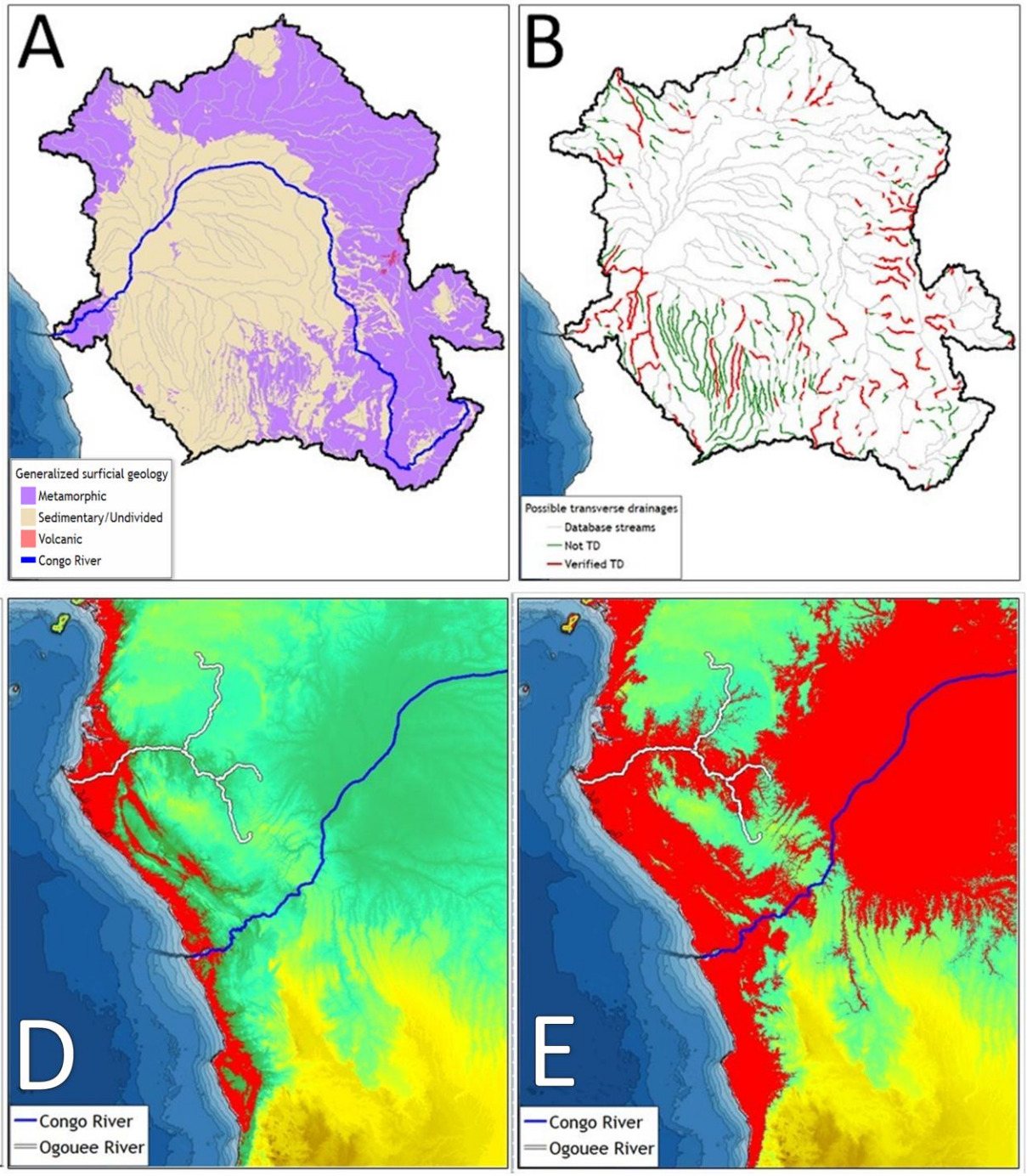
The north-flowing pattern of the tributaries in the eastern part of the basin led Veatch (1935) to speculate that these streams originally continued their north-flowing direction. Other researchers have proposed the past existence of a Megalake Congo, based upon palaeocurrent data (Roberts et al., 2012), the orientation of the major tributaries, and the presence of a submarine canyon rather than a delta at the Congo's mouth (Pound et al., 2013).

One of the most significant features of the Congo watershed is the series of transverse drainages below the Malebo Pool which create the rapids through which the river flows enroute to its outlet in the Atlantic. Since flowing water wants to follow the path of least resistance, the origin of these transverse drainages needs to be integrated into any explanation of the drainage evolution of the Congo River.

Geology

The Congo Basin is a sedimentary basin underlain by Archean to Mesoproterozoic basement which has developed as an intracratonic depression influenced by rifting and subsidence (Braun et al., 2026). The river originates in metamorphic provinces of the Shaba Highlands in the east and flows across the surficial sediments of the central basin, the Cuvette Central. Just before Kinshasa and Brazzaville, it crosses the sandstones of the Bateke Plateau, enters the Malebo Pool, then flows across the Precambrian quartzites and schists of the Crystal Mountains into the Atlantic Ocean (Runge, 2007).

Figure 8. (A–E) Congo basin overview. (A) Simplified geologic map. (B) Locations of possible transverse drainages from database: visually verified TDs in red, negative identifications in green. (C) TDs in adjacent basins; database TDs as solid red lines, non-database transverse streams as dashed red lines. (D) HydroSHEDS DEM with elevations <150 shaded red, showing the oversized delta of the Ogooue and the Congo watershed. (E) HydroSHEDS DEM with elevations <500m shaded red, illustrating the wind gap between the Ogoue and the Congo watersheds, as well as the narrowness of the Congo in its current channel.



Database analysis

There are 123 verified TDs in the Congo watershed, the third largest among all the HydroSHEDS basins. The main HydroSHEDS streamline consists of the combined Luvua and middle and lower Congo Rivers. There are nine TDs on the main trunk and 114 on tributaries.

Verified TDs represent about 45% of all possible TDs in the watershed. This is a very low percentage for the dataset, resulting from the large number of false positives generated by deeply incised channels in the southern plateaus of the basin (Fig 8B).

A notable regional feature is the existence of transverse drainage on rivers in the adjacent coastal basins, including many on streams not in the database (Fig 8C).

Origin theories

Published theories for the origin of the Congo basin's transverse drainage include superimposition, antecedence and stream capture (Table III).

Table III. Proposed theories of origin for the Congo River basin.

Publication year	Author	Evidence - Biologic (B) vs Geologic (G)
ANTECEDENCE		
1999	Karner & Driscoll	G
2015	Flügel et al.	G
STREAM CAPTURE		
1935	Veatch	G
1945	Dixey	G
1954	Cahen	G
1963	Poll	B
1976	Roberts & Stewart	B
1983	Balon & Stewart	B
1997	Lévêque, C	B
1999	Karner & Driscoll	G
2002	Babonneau et al.	G
2003	Lucazeau et al.	G
2004	Key et al.	G
2005	Giresse	G
2005	Goudie	G
2006	Stankiewicz & de Wit	G
2007	Runge	G
2010	Anka et al.	G
2011	Schwarzer et al.	B
2014	Flügel	G
2015	Flügel et al.	G
SUPERIMPOSITION		
1991a-b	Deffontaines & Chorowicz	G
2015	Flügel et al.	G

Stankiewizc and de Wit (2006) argued that the Congo basin was submerged during the Cretaceous, and once it emerged, flowed east into the Indian Ocean. Later, the creation of the East African Rift system tilted the basin to the west. Runge (2007) suggested that the Atlantic Rise during the Pliocene dammed the course of the Congo, leading to the formation of a large lake that survives as the Malebo Pool. Karner and Driscoll (1999) used basin modelling and offshore sequence stratigraphy to suggest that the Congo first flowed into the current path of the Ogouee River, which was later supported by Nibbelink & Budihardjo (2002) based on seismic data. Lucazeau et al. (2003) proposed that the paleo-Congo was endorheic during early Tertiary and that the Ogouee River occupied part of the present-day Congo drainage, which was further supported by Leturmy et al. (2003).

When Karner & Driscoll (1999) first proposed their theory, they did not suggest a cause for the river's migration, but stream capture is the most common cause proposed by other researchers (Table III), consistent with an increasing trend in the literature to credit stream capture for transverse drainage formation, so that it presently accounts for almost 70 percent of the total references in the Appendix database.

Despite its prevalence in the literature, however, the concept of true drainage-head stream capture has been controversial (Lee, 2021):

1. Horton (1945): Proposed the existence of a belt of non-erosion at headward reaches of catchments.
2. Strahler (1945): Considered stream piracy to be contrary to all principles of sound stream behavior, and could not conceive of a small stream having the ability to erode through a resistant divide.
3. Bishop (1995): Questioned drainage-head erosion as a mechanism for stream capture and cautioned against its routine invocation as a mechanism of TD formation.
4. Larson et al. (2017): Maintained that piracy is overutilized in academia and comparatively rare in reality.

Physical constraints on stream capture include the following:

1. Stream piracy experiments have found that symmetric divides hinder the ability of a stream to retreat across the ridge apex, and that the slope across the divide needs to be steep enough compared to the uncaptured stream to prevent deposition occurring across the divide and forming a levee (Douglass and Schmeeckle, 2007)
2. The ability of seepage erosion and groundwater sapping to erode bedrock valleys in resistant rocks is questionable (Lamb et al., 2006; Lamb and Dietrich, 2009; Irwin et al., 2014)
3. Lithology can inhibit knickpoint migration, overriding regional base level control. (See for example, Denn's (2017) finding in a sandstone-underlain catchment in the headwaters of the Appalachian Plateau that knickzones can be hung up in small drainages where hillslope processes influence erosion rates more strongly than fluvial incision, and the stream power model of incision ceases to apply.)
4. Studies of gully formation demonstrate that overland flow is unlikely to breach divides:
    - Experimental evidence has shown that knickpoints decrease in size and rate of migration as they propagate upstream because of reduction in basin area and resulting decrease in discharge, and that at any given flow discharge, headcut development either dissipates or reaches a steady state condition where scour hole geometry, rate of migration, and sediment yield remain unchanged (Bennett et al., 2000; also see the comprehensive summary of knickpoint research in Cantelli and Muto, 2014)
    - Gully channel formation is very intense during the period of gully initiation, but during the last and largest portion of a gully's lifetime, the gully is morphologically near stable (Magilligan & Stamp (1997), and Sidorchuk (1999), describing the experiments of Kosov et al. (1978))
    - Soil type and vegetation can both reduce the erodibility of natural systems, including drainage divides (Kleinhans et al., 2014; Torri and Poesen, 2014).

Negative evidence against stream capture as the cause of the shift of the Congo River to its current location

Physical constraints of the Lower Congo channel below the Malebo Pool. During the first 150 km, a capturing stream would have had to breach the folded and deformed West Congolian Supergroup (Tack et al., 2001), including at least five 90 degree turns (Fig 9B). Once the proposed headward-eroding stream breached those lithologies, it would then have had to erode about 120 km upstream through the arkosic sandstones of the Inkisi Group (Tack et al., 2001), creating a channel that is so narrow, the current flow is often concentrated in a jet (Oberg et al., 2009). It is difficult to envision how the stream capture mechanisms of mass wasting, in situ weathering, rain splash, sheetwash, knickpoint recession, and groundwater sapping, could have eroded such twists and turns through the ridges and finally created a deep and narrow channel in such resistant lithology. Water flowing over an impoundment, however, is very capable of carving channels through cavitation processes. For example, in 2017 at the Oroville Dam in Oroville, California, high-flow releases over a small crack in the concrete of the main spillway triggered massive cavitation forces that destroyed the rest of the chute (Independent Forensic Team, 2018).

In addition, two database tributaries and two non-database tributaries of the lower Congo clearly exhibit TDs (Fig. 9B). Under the stream capture hypothesis, a stream eroding headward from the Atlantic would have had to have diverged at least four times at each tributary junction, and each branch would then have eroded headward in different directions. As above, given the mechanisms proposed for stream capture, it is difficult to envision this happening.

Complexity of the drainage network above the Malebo Pool within the Bateke Plateau. The Congo and its chief southern tributary, the Kasai, both flow in transverse drainages across the Bateke Plateau before joining about 140 km upstream of the Malebo Pool (Fig 9C). Under a stream capture scenario, this means that once a proposed Atlantic-flowing stream eroded through the Crystal Mountains, it would still have had to erode through the Malebo Pool (assuming it existed at the time) and the Bateke Plateau, then diverge into two channels about 140 km upstream of the Pool.

In addition to the Kasai, there are two tributaries that join the Congo through TDs in the Bateke Plateau above the Malebo Pool and one that flows through a TD directly into the Pool. Another stream flows north through the plateau before turning 90 degrees east to flow through a TD on its way to join the Kasai. (Fig. 9C). Under a stream capture scenario, this would require that either:

- The original Atlantic-flowing stream diverged within the Malebo Pool, then at least three times upstream of the pool, or
- Four streams eroded headward through the plateau, then made abrupt 90 degree turns to flow through TDs on their way to join the main trunk or the Malebo Pool (Fig. 9C).

Proposed overflow scenario

Original paleogeography and basin formation. The Congo originally flowed east (Stankiewicz & De Wit, 2006). The rise of the East African Rift cut off the east-flowing drainage and formed an endorheic basin, which is supported by the presence of lacustrine sediments in the basin (Giresse, 2005; Stankiewicz & De Wit, 2006; Runge, 2007; Schwarzer et al., 2011; Caillaud et al., 2017). This resulted in the highest elevations around the Basin being in the eastern mountains, while the western boundary is formed by the largely level Bateke Plateau, which is highly dissected by Congo tributaries flowing into the Cuvette Central and by Atlantic-draining streams flowing away from the basin divide.

Possible Megalake Congo. The presence of a megalake within the Congo basin has been proposed before (Cahen, 1954; Pound et al., 2013), but there are no studies explicitly mapping paleoshorelines similar to those of Lake Chad to the north and Kalahari Megalake Makgadikgadi to the south (Drake & Bristow, 2006; Burrough et al., 2009). However, examination of the SRTM DEM used in this study suggests that contour levels between 330-360 m within the basin may represent shorelines of a previously unreported multi-lobed paleolake within the Congo Basin, from which the two transverse drainages from the Congo and the Kasai extend across the Bateke Plateau (Fig (9A). Interestingly, Lake Chad, to the north has a well-documented paleolake shoreline around 330 m asl (Quade et al., 2018) and also exhibits a small ~70 km long transverse drainage at its outlet to the Niger River, which currently functions as a spillway (Mémin et al., 2020). Unlike Lake Chad and Megalake Makgadikgadi, however, the Congo Basin has a densely forested interior, and ground-truthed evidence of actual paleo-shorelines may be difficult to achieve.

Wind gaps indicating older outlets. At least part of the basin experienced overflow through the current path of the Ogouee River (Karner & Driscoll, 1999; Nibbelink & Budihardjo, 2002). This is supported by the oversize delta of the Ogouee (Flügel, et al., 2015; Fig. 8C) and by wind gaps between Congo and Ogouee tributaries (Fig. 9D-E).

Other possible Atlantic-draining paleoflows include clearly defined wind gaps on the Bateke Plateau between northeast-flowing Congo tributaries and southwest-flowing tributaries of the Atlantic-draining Kouilou River. (Fig. 9D).

Stankiewicz & De Wit (2006) noted two basin-wide surfaces within the Cuvette Centrale at 457 m and 610 m. The low points on the two northernmost Ogouee wind gaps are at 473 m, so they could represent overflow from the 457 m surface, while the other wind gaps on the Bateke Plateau range from 537-630 m (average = 600 m) and could represent former overflow paths from the 610 m surface. Since both the Ogouee and

Bateke Plateau wind gaps are higher than the possible paleolake shorelines of 330-360 m, any paleoflow through them would have occurred prior to establishment of the proposed paleolake.

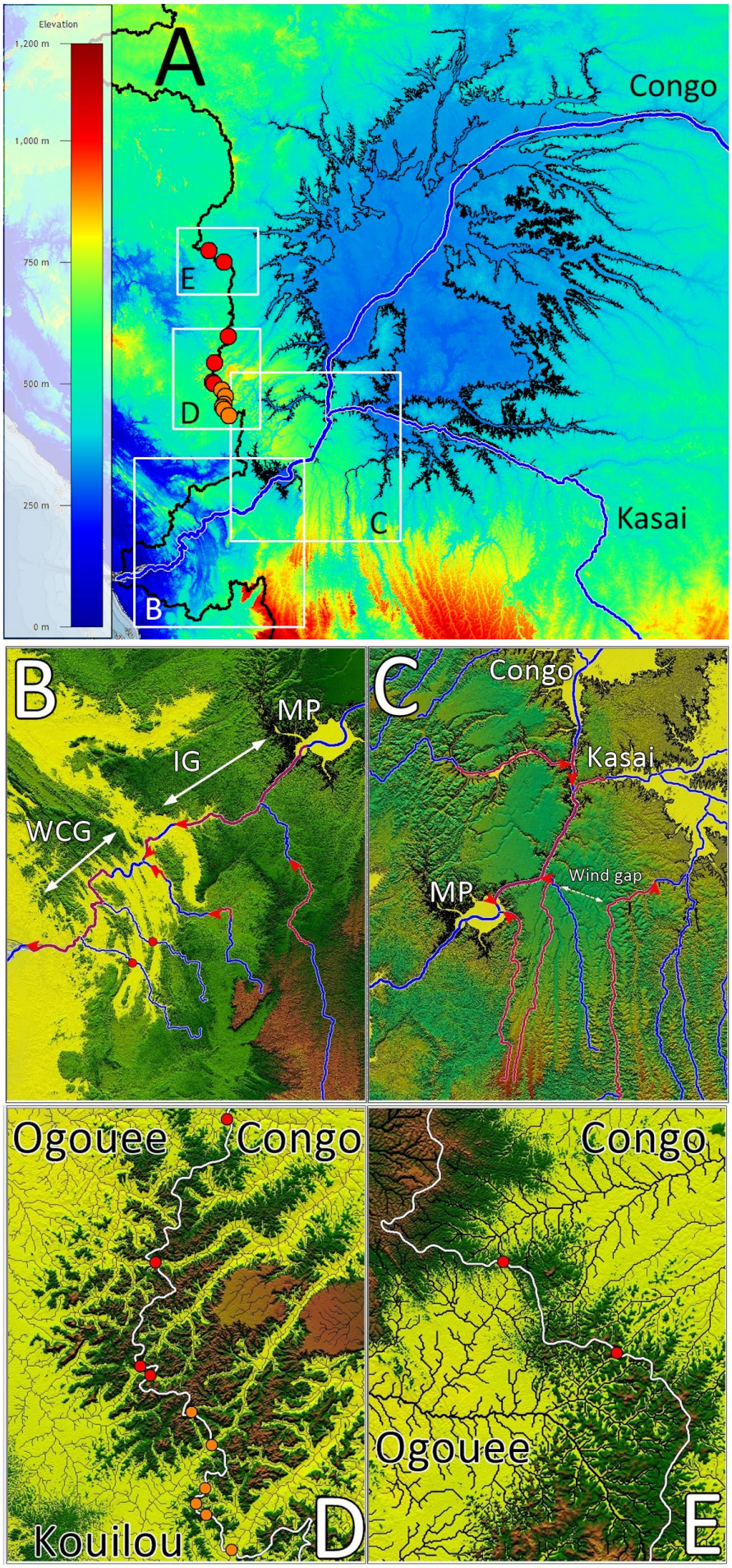
The morphology of the Congo-Ogouee-Kouilou wind gaps and the current channel are consistent with Douglass and Schmeeckle's (2007) stream experiments, which demonstrated that, given two or more outlets from an overflowing basin, one will erode faster, leaving the others as wind gaps. The northernmost Ogouee wind gaps are on a low saddle along the divide (Fig. 8E), and along with the Bateke Plateau wind gaps, should represent previous outflows from the post-rifting, tilted Congo basin before the outlet was created across the Bateke Plateau to the Malebo Pool. (Fig 9D-E). Oberg et al. (2009) pointed out that the lower Congo's channel is more like a high-gradient mountain stream with a large discharge and is much deeper and narrower in its lower reaches than expected for a river of its size. In other large rivers like the Parana and the Mississippi, the channel width divided by the mean depth is usually larger downstream than upstream, whereas the reverse is true for the Congo (Oberg et al., 2009).

Tectonic triggers and hydraulic mechanics of the current shift. Nkodia et al (2020a, 2020b) described still active strike-slip fault systems in the Lower Congo arkoses of the Inkisi group downstream from the Malebo Pool with a compression direction of N078^{o} and suggested ridge push from the Atlantic Ocean as a mechanism. In 2024, the same researchers specifically linked reactivation of pre-existing faults to the connection of the Congo to the Atlantic coast in the Oligocene period (Nkodia et al., 2024). While they follow previous researchers in attributing the drainage change to stream capture, the Inkisi Group underlies the formations of the Bateke Plateau (Nkodia et al., 2020a), so it is not inconceivable that seismic activity could have activated new and/or pre-existing fractures in the Bateke Plateau, allowing mechanisms such as seepage and piping to redirect drainage into the Malebo Pool. In this model, the proposed paleolake at 330-360 m represents a lake dammed by the Bateke Plateau which was fractured by seismic activity, causing catastrophic overflow through the current outlet to the Atlantic.

While many documented overflow locations are through ridges, for example, Lake Bonneville through Red Rock Pass, Utah, US, (Sack, 1999; Hilgendorf et al., 2020), overflow over plateaus is not unknown. One spectacular example is the proposed overflow of Lake Bidahochi across the Kaibab Plateau to form the Grand Canyon in Arizona, US (Douglass et al., 2020; He et al., 2026).

Figure 9. Congo Basin. (A) Congo basin overview. Boxes indicate figures 9D-E. Thin black lines indicate possible paleshorelines at 330 m and 360 m, thick line is basin boundary. Red dots are wind gaps with Ogouee River, orange dots are wind gaps with Kouilou River. (B) Lower Congo and tributaries, elevations shaded yellow below 330 m for contrast. Red arrows are database TDs, red dots are TDs on non-database streams. WCG: West Congolian Group; IG: Inkisi Group; MP: Malebo Pool. (C) TDs of Congo, Kasai, and other Congo tributaries at Malebo Pool and Bateke Plateau, elevations below 330 m shaded yellow. (D) Wind gaps between Ogouee (red dots)/ Kouilou (orange dots) and Congo River on the Bateke Plateau, elevations under 610 m

shaded yellow. (E) Wind gaps between Ogouee and Congo tributaries, elevations under 480 m shaded yellow.


Elevation
1,200 m
1,000 m
750 m
500 m
250 m
0 m
A
Congo
Kasai
E
D
C
B
B
MP
IG
WCG
C
Congo
Kasai
Wind gap
MP
Ogouee
Congo
Kouilou
D
Congo
Ogouee
E

The geomorphological evidence is negative for stream capture, while supporting overflow for the formation of transverse drainages on the lower Congo. The initiating event for an overflow could have been tectonic movements, perhaps related to the creation of the Malebo Pool (Nkodia et al., 2024). However, the large number of TDs in the basins adjacent to the Congo (Fig 8C) indicates that transverse drainage was a regional event. More research is needed to better constrain the causes and processes involved in the river's shift.

DIRECTIONS FOR FUTURE STUDY

Expanding the methodology to RiverATLAS streams less than 200 km long would create a comprehensive worldwide database of transverse drainages. Additionally, the ubiquity of TDs along the northwest Pacific coast, the east coast of Brazil and the southwest coast of Africa offers possibilities for future investigation. Studies have shown that knickzones on river profiles, on a continental scale, are not dependent on lithological contacts, and that there is a conflict between the complex, non-linear fluid dynamics of channel evolution and the apparent simplicity of emergent continental-scale landforms (Fernandes et al., 2019; Roberts et al., 2019). In North America, for example, Fernandes et al. (2019) found that North American rivers flow radially from large-scale swells, with wavelengths of the order 100-1000 km, and the data from this study demonstrates that transverse drainages are an integral part of many of those rivers. Examination of the relationship of large-scale transverse drainages to large-scale continental river profiles could be a fruitful path of investigation into the history of the Earth's uplift and denudation.

CONCLUSION

The existence of transverse drainages in a river basin has important implications for its history, and on a larger scale, for the history of uplift and denudation of continents. From a practical perspective, river managers need to understand a basin's history over geologic and human time scales because a given river's response potential will be governed in part by prior disturbance history (Buffington & Montgomery, 2021).

The methodology presented here demonstrates the use of a terrain filtering methodology for systematically identifying and mapping discordant river patterns at many scales across the globe, revealing previously unreported TDs in various regions and providing insights into their global distribution and physical characteristics. It can filter thousands of streams for possible transverse drainages, is customizable for the needs of any given region, and integrates digital elevation models and spatial databases with modern graphic visualization platforms. The analysis of the Congo basin shows the capability of refined DEMs and data extraction models such as the methodology described here for more intensive and in-depth exploration of the earth's surface.

The study also points out the current limits of the use of artificial intelligence in geological research. The necessity of visual confirmation for final TD identification demonstrates that in the area of three-dimensional analysis, AI and algorithms can help filter large quantities of data, but human intelligence is still required for final verification.

References

Anka Z, Ondrak R and Schulz HM (2010) Evidence of a large upper-cretaceous depocentre across the Continent-Ocean boundary of the Congo-Angola basin: implications for palaeo-drainage and potential ultra-deep source rocks. Marine and Petroleum Geology 27: 797-814.

Arzhannikov SG, Ivanov AV, Arzhannikova AV, et al. (2017) Catastrophic events in the Quaternary outflow history of Lake Baikal. Earth-Science Reviews 177: 76-113.

Babonneau N, Veiga I, Savoye B, et al. (2002) Morphology and architecture of the present canyon and channel system of the Zaire deep-sea fan. Marine and Petroleum Geology 19: 445-467.

Bally AL (2007) Tectonic Map of the World [GIS dataset]. American Association of Petroleum Geologists. Tectonic Map of the World, 2007 Datapages.

Balon EK and Stewart DJ (1983) Fish assemblages in a river with unusual gradient (Luongo, Africa-Zaire system), reflections on river zonation, and description of another new species. Environmental Biology of Fishes 9: 225-252.

Batbaatar J and Gillespie AR (2015) Outburst floods of the Maly Yenisei. Part I. International Geology Review 58: 1723-1752.

Batchelor CL, Margold M, Krapp M, et al. (2019) The configuration of Northern Hemisphere ice sheets through the Quaternary. Nature Communications 10: 3713.

Bennett SJ, Alonso CV, Prasad SN, et al. (2000) Experiments on headcut growth and migration in concentrated flows typical of upland areas. Water Resources Research 36: 1911-1922.

Bishop P (1995) Drainage rearrangement by river capture, beheading and diversion. Progress in Physical Geography: Earth and Environment 19: 449-473.

Bloom AL (1998) Geomorphology: A Systematic Analysis of Late Cenozoic Landforms. 3rd edition. Prentice Hall.

Bracciali L, Najman Y, Parrish RR, et al. (2015) The Brahmaputra tale of tectonics and erosion: early Miocene river capture in the Eastern Himalaya. Earth and Planetary Science Letters 415: 25-37.

Brardinoni F and Hassan MA (2006) Glacial erosion, evolution of river long profiles, and the organization of process domains in mountain drainage basins of coastal British Columbia. Journal of Geophysical Research, Earth Surface 111: F01013.

Braun JJ, Kadima Kabongo E, Audry S, et al. (2026) Geology and geodynamics evolution of the Congo Basin Resilience and Sustainability in the Congo Basin: Retracing the Past, Looking to the Future. Springer, pp. 1-38.

Buffington JM and Montgomery DR (2021) Geomorphic classification of Rivers: an updated review. In: Treatise on Geomorphology. 2nd edition. Elsevier, pp. 1143-1190.

Burbank DW, Leland J, Fielding E, et al. (1996) Bedrock incision, rock uplift and threshold hillslopes in the Northwestern Himalayas. Nature 379: 505-510.

Burrough SL, Thomas DS and Bailey RM (2009) Mega-Lake in the Kalahari: a late Pleistocene record of the Palaeolake Makgadikgadi system. Quaternary Science Reviews 28: 1392-1411.

Cahen L (1954) Géologie du Congo Belge. Vaillant-Carmanne.

Caillaud A, Blanpied C and Delvaux D (2017) The Upper Jurassic Stanleyville group of the Eastern Congo Basin: an example of perennial lacustrine system. Journal of African Earth Sciences 132: 80-98.

Cantelli A and Muto T (2014) Multiple knickpoints in an alluvial river generated by a single instantaneous drop in base level: experimental investigation. Earth Surface Dynamics 2: 271-278.

Clark GM (1989) Central and southern Appalachian water and wind gap origins: review and new data. Geomorphology 2: 209-232.

Coe D and Wolfe E (2016) Floodplain visualization using LiDAR derived relative elevation models - Natural systems design. (Accessed 8 March, 2025).

Deffontaines B and Chorowicz J (1991a) Principles of drainage basin and river network analysis by slope-facet mapping, for application to neotectonics. International Journal of Remote Sensing 12: 2431-2456.

Deffontaines B and Chorowicz J (1991b) Principles of drainage basin analysis from multisource data: application to the structural analysis of the Zaire Basin. Tectonophysics 194: 237-263.

Denn AR (2017) Detecting Landscape Response to Perturbations by Climate and Base Level in Central Pennsylvania Using In-Situ 10Be and 26Al. Master's thesis. University of Vermont.

Dixey F (1945) The Ladysmith Basin. South African Geographical Journal 27: 33-43.

Douglass J and Schmeeckle M (2007) Analogue modeling of transverse drainage mechanisms. Geomorphology 84: 22-43.

Douglass J, Meek N, Dorn RI, et al. (2009) A criteria-based methodology for determining the mechanism of transverse drainage development, with application to the Southwestern United States. Geological Society of America Bulletin 121: 586-598.

Douglass JC, Gootee BF, Dallegge T, et al. (2020) Evidence for the overflow origin of the Grand Canyon. Geomorphology 369: 107361.

Drake N and Bristow C (2006) Shorelines in the Sahara: geomorphological evidence for an enhanced monsoon from Palaeolake Megachad. The Holocene 16: 901-911.

Ehlers J, Gibbard PL and Hughes PD (eds) (2011) Quaternary Glaciations - Extent and Chronology: A Closer Look

(Developments in Quaternary Science). Elsevier, Vol. 15.

Fernandes VM, Roberts GG, White N, et al. (2019) Continental-scale landscape evolution: a history of North American topography. Journal of Geophysical Research, Earth Surface 124: 2689-2722.

Flügel TJ (2014) The Evolution of the Congo-Kasai Drainage System. Doctoral dissertation, University of the Witwatersrand.

Flügel TJ, Eckardt FD and Cotterill FP (2015) The present day drainage patterns of the Congo River system and their Neogene evolution. In: de Wit MJ, Guillocheau F and de Wit MCJ (eds) Geology and Resource Potential of the Congo Basin. Springer, pp. 315-337.

Geological Survey US (2014) Shuttle Radar Topography Mission (SRTM) 1 Arc-Second Global. [Dataset]. (Accessed March, 2026).

Giresse P (2005) Mesozoic-cenozoic history of the Congo Basin. Journal of African Earth Sciences 43: 301-315.

Gorelick N, Hancher M, Dixon M, et al. (2017) Google Earth engine: planetary-scale geospatial analysis for everyone. Remote Sensing of Environment 202: 18-27.

Goudie AS (2005) The drainage of Africa since the Cretaceous. Geomorphology 67: 437-456.

Greco SE, Girvetz EH, Larsen EW, et al. (2008) Relative elevation topographic surface modelling of a large alluvial river floodplain and applications for the study and management of riparian landscapes. Landscape Research 33: 461-486.

Hall K (2022) Last Glacial Maximum (Item ID: 046cde34ce804141a8d5303656e74f44) [Feature layer]. ArcGIS Online. (Accessed 17 August 2026).

Harrison IJ, Brummett R and Stiassny ML (2016) The Congo River Basin. In: Finlayson CM, Milton GR, Prentice RC, et al. (eds) The Wetland Book. Springer, pp. 845-856.

Hartmann J and Moosdorf N (2012) The new global lithological map database GLIM: a representation of rock properties at the Earth surface. Geochemistry, Geophysics, Geosystems 13: Q12004.

He JJ, Crow RS, Douglass J, et al. (2026) Late Miocene Colorado River arrival in the Bidahochi basin supports spillover origin of Grand Canyon. Science 392: 289-295.

Heins WA (2023) Honest bookkeeping for source-to-sink sediment mass-balance analysis with examples from the Angoche margin of Mozambique and the Corsica trough of France. Marine and Petroleum Geology 153: 106265.

Herget J (2005) Reconstruction of Pleistocene Ice-Dammed Lake Outburst Floods in the Altai Mountains, Siberia. Geological Society of America.

Hilgendorf Z, Wells G, Larson PH, et al. (2020) From basins to rivers: understanding the revitalization and significance of top-down drainage integration mechanisms in drainage basin evolution. Geomorphology 352: 107020.

Hill CA, Eberz N and Buecher RH (2008) A karst connection model for Grand Canyon, Arizona, USA. Geomorphology 95: 316-334.

Horton RE (1945) Erosional development of streams and their drainage basins; hydrophysical approach to quantitative morphology. Geological Society of America Bulletin 56: 275-370.

Independent Forensic Team (2018) Independent Forensic Team Report: Oroville Dam Spillway Incident. California Department of Water Resources.

Irwin RP, Tooth S, Craddock RA, et al. (2014) Origin and development of theater-headed valleys in the Atacama Desert, northern Chile: morphological analogs to Martian valley networks. Icarus 243: 296-310.

Jackson PR, Oberg KA, Gardiner N, et al. (2009) Velocity mapping in the lower Congo River: a first look at the unique bathymetry and hydrodynamics of Bulu Reach, West Central Africa. In: Proceedings of the IAHR Symposium on River Coastal and Estuarine. Morphodynamics, Santa Fe, Argentina, 2009, Vol. 6, pp. 1007-1014.

Kadima E, Delvaux D, Sebagenzi SN, et al. (2011) Structure and geological history of the Congo Basin: an integrated interpretation of gravity, magnetic and reflection seismic data. Basin Research 23: 499-527.

Karner GD and Driscoll NW (1999) Tectonic and stratigraphic development of the West African and eastern Brazilian Margins: insights from quantitative basin modelling. Geological Society, London, Special Publications 153: 11-40.

Key RM, De Waele B and Liyungu AK (2004) A multi-element baseline geochemical database from the Western extension of the Central Africa Copperbelt in northwestern Zambia. Applied Earth Science 113: 205-226.

Kleinhans MG, van Dijk WM, van de Lageweg WI, et al. (2014) Quantifiable effectiveness of experimental scaling of river- and delta morphodynamics and stratigraphy. Earth-Science Reviews 133: 43-61.

Kosov B, Nikol'skaya I and Zorina YF (1978) Eksperimental'nyye issledovaniya ovragoobrazovaniya. Eksposisi Geomorfologi 3: 113-140.

Labaš P, Kidová A and Afzali H (2024) Using the relative elevation models to delimit the floodplain level development: the case of the braided-wandering Belá River, Slovakia. Moravian Geographical Reports 32: 187-200.

Lajeunesse P (2014) Buried preglacial fluvial gorges and valleys preserved through Quaternary glaciations beneath the eastern Laurentide Ice Sheet. Geological Society of America Bulletin 126: 447-458.

Lamb MP and Dietrich WE (2009) The persistence of waterfalls in fractured rock. Geological Society of America Bulletin 121: 1123-1134.

Lamb MP, Howard AD, Johnson J, et al. (2006) Can springs cut canyons into rock? Journal of Geophysical Research 111: E7.

Larson PH, Meek N, Douglass J, et al. (2017) How rivers get across mountains: transverse drainages. Annals of the Association of American Geographers 107: 274-283.

Lee J (2013) A survey of transverse drainages in the Susquehanna River basin, Pennsylvania. Geomorphology 186: 50-67.

Lee J (2019) A global database of large-scale transverse drainages. Data in Brief 23: 103650.

Lee J (2021) Giant gorges, colossal canyons and vast valleys: evaluating mechanisms of formation for a set of Large-scale transverse drainages. SSRN Electronic Journal.

Lehner B and Grill G (2013) Global river hydrography and network routing: baseline data and new approaches to study the world's large river systems. Hydrological Processes 27: 2171-2186.

Leturmy P, Lucazeau F and Brigaud F (2003) Dynamic interactions between the Gulf of Guinea passive margin and the Congo River drainage basin: 1. Morphology and mass balance. Journal of Geophysical Research: Solid Earth 108: 2384.

Leturmy P, Lucazeau F and Brigaud F (2003) Dynamic interactions between the Gulf of Guinea passive margin and the Congo River drainage basin: 1. Morphology and mass balance. Journal of Geophysical Research: Solid Earth, 108(B8).

Lévêque C (1997) Biodiversity Dynamics and Conservation: The Freshwater Fish of Africa. Cambridge University Press.

Linke S, Lehner B, Dallaire CO, et al. (2019) Global hydro-environmental sub-basin and river reach characteristics at high spatial resolution. Scientific Data 6: 283.

Magilligan FJ and Stamp ML (1997) Historical land-cover changes and hydrogeomorphic adjustment in a small Georgia watershed. Annals of the Association of American Geographers 87: 614-635.

Margold M, Jansen JD, Codilean AT, et al. (2018) Repeated megafloods from glacial Lake Vitim, Siberia, to the Arctic Ocean over the past 60,000 years. Quaternary Science Reviews 187: 41-61.

Master S (2010) Lac Télé structure, Republic of Congo: geological setting of a cryptozoological and biodiversity hotspot, and evidence against an impact origin. Journal of African Earth Sciences 58: 667-679.

Medlicott HB (1879) A Manual of the Geology of India: Chiefly Compiled from the Observations of the Geological Survey. Peninsular Area. Geological Survey Office.

Mémin A, Ghienne JF, Hinderer J, et al. (2020) The hydro-isostatic rebound related to megalake Chad (Holocene, Africa): first numerical modelling and significance for paleo-shorelines elevation. Water 12: 3180.

Monegato G, Massironi M and Martellato E (2010) The ring structure of Wembo-Nyama (Eastern Kasai, RD Congo): a possible impact crater in Central Africa. In: 41st Annual Lunar and Planetary Science Conference, Woodlands, Texas, 1-5 March, 2010, p. 1601.

Morisawa M (1989) Rivers and valleys of Pennsylvania, revisited. Geomorphology 2: 1-22.

National Centers for Environmental Information (NCEI) (2022) ETOPO 2022 15 ARC-Second Global Relief Model. NOAA National Centers for Environmental Information. (Accessed 15 July, 2025).

Ni Y, Wang H, Xu H, et al. (2024) Relative elevation modelling of Linyi district and applications for the study of active faults. In: Third International Conference on Remote Sensing, Surveying and Mapping (RSSM 2024), Wuhan, China, 12-14 January, 2024.

Nibbelink K and Budihardjo S (2002) Paleo-Congo River fan in Northern Gabon. In: Paper presented at the AAPG Annual Meeting, Houston, TX, 10-13 March, 2002.

Nkodia HMD, Miyouna T, Delvaux D, et al. (2020a) Neotectonics of Brazzaville and Kinshasa: linking Congo Basin seismicity and in situ stress in the Inkisi Group. Solid Earth Preprint.

Nkodia HMDV, Miyouna T, Delvaux D, et al. (2020b) Flower structures in sandstones of the Paleozoic Inkisi Group (Brazzaville, Republic of Congo): evidence for two major strike-slip fault systems and geodynamic implications. South African Journal of Geology 123: 531-550.

Nkodia HMD, Boudzoumou F, Miyouma T, et al. (2024) Brittle faulting and tectonic stress history on the Western margin of the Congo Basin between Kinshasa and Brazzaville: implications for the evolution of the Malebo Pool and the Congo River. Tectonophysics 877: 230282.

Oberg KA, Shelton JM, Gardiner N, et al. (2009) Discharge and other hydraulic measurements for characterizing the hydraulics of Lower Congo River, July 2008. In: Proceedings of the 33rd IAHR Congress: Water Engineering for a Sustainable Environment. International Association for Hydro-Environment Engineering and Research. pp. 4486-4493.

Olson PL, Legg NT, Abbe TB, et al. (2014) A Methodology for Delineating planning-level Channel Migration Zones. Washington State Department of Ecology Publication No. 14-06-025.

OpenTopography (2022) New package automates river relative elevation model (REM) generation. (Accessed 8 March, 2025).

Owen J and Caslys Consulting (2024) Floodplain Visualization with Relative Earth Models. (Accessed 8 March, 2025).

Pederson DT (2001) Stream piracy revisited: a groundwater-sapping solution. GSA Today 11: 4-10.

Pham JP (2014) In Congo, Third Time's No Charm. The Hill. (Accessed 21 April, 2026).

Poll M (1963) Zoogéographie ichthyologique du cours supérieur du Lualaba. Publ. Univ. État Élisabethville 6: 95-106.

Poole GC, Stanford JA, Frissell CA, et al. (2002) Three-dimensional mapping of geomorphic controls on flood-plain hydrology and connectivity from aerial photos. Geomorphology 48: 329-347.

Pound MJ, Tindall J, Pickering SJ, et al. (2013) Late Pliocene lakes and soils: a data-model comparison for the analysis of climate feedbacks in a warmer world. Climate of the Past Discussion 9: 3175-3207.

Quade J, Dente E, Armon M, et al. (2018) Megalakes in the Sahara? A review. Quaternary Research 90: 253-275.

Roberts TR and Stewart DJ (1976) An ecological and systematic study of the fishes in the rapids of the lower

Zaire or Congo River. Bulletin of the Museum of Comparative Zoology 147: 239-317.

Roberts EM, Stevens NJ, O'Connor PM, et al. (2012) Initiation of the Western branch of the East African Rift coeval with the Eastern branch. Nature Geoscience 5: 289-294.

Roberts GG, White N and Lodhia BH (2019) The generation and scaling of longitudinal river profiles. Journal of Geophysical Research, Earth Surface 124: 137-153.

Runge J (2007) The Congo River, Central Africa. In: Gupta A (ed) Large Rivers: Geomorphology and Management. John Wiley & Sons, Ltd, pp. 293-309.

Sack D (1999) The composite nature of the Provo level of Lake Bonneville, Great Basin, Western North America. Quaternary Research 52: 316-327.

Schwarzer J, Misof B, Ifuta SN, et al. (2011) Time and origin of cichlid colonization of the Lower Congo Rapids. PLoS One 6: e22380.

Shinn J (2015) Relative Elevation Surface Model for the Shasta River, CA. Data Basin. (Accessed 8 March, 2025).

Sidorchuk A (1999) Dynamic and static models of gully erosion. Catena 37: 401-414.

Stankiewicz J and de Wit MJ (2006) A proposed drainage evolution of the Congo basin since the breakup of Gondwana. South African Journal of Geology 109: 487-508.

Stokes M, Mather AE, Belfoul A, et al. (2008) Active and passive tectonic controls for transverse drainage and river gorge development in a collisional mountain belt (Dades Gorges, High Atlas Mountains, Morocco). Geomorphology 102: 2-20.

Strahler AN (1945) Hypotheses of stream development in the folded Appalachians of Pennsylvania. Geological Society of America Bulletin 56: 45-88.

Tack L, Wingate MTD, Liégeois JP, et al. (2001) Early Neoproterozoic magmatism (1000-910 Ma) of the Zadinian and Mayumbian Groups (Bas-Congo): onset of Rodinia rifting at the Western edge of the Congo craton. Precambrian Research 110: 277-306.

Torri D and Poesen J (2014) A review of topographic threshold conditions for gully head development in different environments. Earth-Science Reviews 130: 73-85.

Twidale CR (2004) River patterns and their meaning. Earth-Science Reviews 67: 159-218.

Veatch AC (1935) Evolution of the Congo Basin. Geological Society of America Memoirs. Geological Society of America 3: 1-183.

Wang S, Haralick RM and Campbell J (1984) Relative elevation determination from Landsat imagery. Photogrammetria 39: 193-215.

World Bank Group (2021) Climate Risk Country Profile: Congo, Democratic Republic. World Bank Group.

Yamazaki D, Ikeshima D, Sosa J, et al. (2019) MERIT Hydro: A high-resolution global hydrography map based on

latest topography dataset. Water Resources Research 55(6): 5053-5073.